

**PERCEIVED QUALITY ASSESSMENT IN
OBJECT-SPACE FOR ANIMATED 3D
MODELS**

A THESIS

SUBMITTED TO THE DEPARTMENT OF COMPUTER ENGINEERING
AND THE GRADUATE SCHOOL OF ENGINEERING AND SCIENCE
OF BILKENT UNIVERSITY

IN PARTIAL FULFILLMENT OF THE REQUIREMENTS
FOR THE DEGREE OF
MASTER OF SCIENCE

By

Işıl Doğa Yakut

June, 2012

I certify that I have read this thesis and that in my opinion it is fully adequate, in scope and in quality, as a thesis for the degree of Master of Science.

Assist. Dr. Tolga apın(Advisor)

I certify that I have read this thesis and that in my opinion it is fully adequate, in scope and in quality, as a thesis for the degree of Master of Science.

Prof. Dr. Bülent Özgüç

I certify that I have read this thesis and that in my opinion it is fully adequate, in scope and in quality, as a thesis for the degree of Master of Science.

Assist. Prof. Dr. Ahmet Oğuz Akyüz

Approved for the Graduate School of Engineering and
Science:

Prof. Dr. Levent Onural
Director of the Graduate School

ABSTRACT

PERCEIVED QUALITY ASSESSMENT IN OBJECT-SPACE FOR ANIMATED 3D MODELS

Işıl Doğa Yakut

M.S. in Computer Engineering

Supervisor: Assist. Dr. Tolga Çapın

June, 2012

Computational models and methods to handle 3D graphics objects continue to emerge with the wide-range use of 3D models and rapid development of computer graphics technology. Many 3D model modification methods exist to improve computation and transfer time of 3D models in real-time computer graphics applications. Providing user with the least visually-deformed model is essential for 3D modification tasks.

In this thesis, we propose a method to estimate the visually perceived differences on animated 3D models. The model makes use of Human Visual System models to mimic visual perception. It can also be used to generate a 3D sensitivity map for a model to act as a guide during the application of modifications.

Our approach gives a perceived quality measure using 3D geometric representation by incorporating two factors of Human Visual System (HVS) that contribute to perception of differences. First, spatial processing of human vision model enables us to predict deformations on the surface. Secondly, temporal effects of animation velocity are predicted. Psychophysical experiment data is used for both of these HVS models. We used subjective experiments to verify the validity of our proposed method.

Keywords: Applied Perceptual Computer Graphics, Quality Evaluation for 3D Model, Animated 3D Models, Computational Geometry.

ÖZET

HAREKETLİ 3B MODELLERİN ALGILANAN KALİTE ÖLÇÜMÜ

Işıl Doğa Yakut

Bilgisayar Mühendisliği, Yüksek Lisans

Tez Yöneticisi: Assist. Dr. Tolga Çapın

Haziran, 2012

Bilgisayar grafiği teknolojisinin hızlı gelişimi ve 3B modellerin yaygın kullanımıyla birlikte 3B grafik nesnelerini kullanan hesaplamalı model ve yöntemler de gelişmeye devam etmektedir. Gerçek zamanlı bilgisayar grafiği uygulamalarında, hesaplama ve aktarım süresini geliştirmek için birçok 3B model modifikasyon yöntemi bulunmaktadır. 3B modifikasyon işlemlerinde, kullanıcıya modelin görsel olarak en az deforme olmuş halini sunmak gerekmektedir.

Bu tez kapsamında, hareketli 3B modeller üzerinde görsel olarak algılanan farklılıkları hesaplamak için bir yöntem sunulmaktadır. Yöntem, insan görme sistemini, görsel algıyı taklit ederek modellemektedir. Ayrıca bu yöntem, modifikasyonların uygulanması sırasında yardımcı olması amacıyla modelin 3B duyarlılık haritasının oluşturulmasında da kullanılabilir.

Bu çalışmada sunulan yaklaşım, İnsan Görme Sistemi'nin iki etmenini birleştirerek 3B geometrik gösterimin algılanan kalite ölçümünü sağlamaktadır. Birincisi, insan görme modelinin uzamsal işlenmesi, yüzeydeki bozulmaları öngörmeyi mümkün kılmaktadır. İkincisi ise, hareket hızının zamansal etkileridir. Her iki etmen için de psikofizik deney verileri kullanılmıştır. Ayrıca kişiye özel deneyler ile de sunulan yöntemin geçerliliği desteklenmiştir.

Anahtar sözcükler: Uygulamalı Algısal Bilgisayar Grafikleri, Üç Boyutlu Modellerde Kalite Belirlenmesi, Hareketli Üç Boyutlu Modelleme, Hesaplamalı Geometry.

Acknowledgement

Foremost, I would like to express my gratitude to my supervisor Assist. Prof. Dr. Tolga apın for his motivation, guidance and patience. His support and kindness helped me in all of the research and writing of my thesis. Besides my advisor, I would like to thank the rest of my thesis committee: Prof. Dr. Bülent Özgüç and Assist. Prof. Dr. Ahmet Oğuz Akyüz for their interest in the subject and their time spent.

I would like to thank to TUBITAK-BIDEB “ALGI” Project and EU 7th Framework “All 3D Imaging Phone” Project for the financial support during my M.Sc. study.

I also thank my lab friends Cansın Yıldız, Abdullah Bülbül and Bengü Kevingç for their support and making time more enjoyable.

Lastly, I am especially grateful to my family. I thank my father for his neverending support, wisdom and kindness, and my mother for enabling a hopeful, loving and peaceful view of life. My sister İdil and my husband Sefa gave me strength with their constant support, encouragement, enthusiasm and calming voice of reason.

Contents

- 1 Introduction** **1**

- 2 Related Work & Background** **5**
 - 2.1 Related Work: Mesh Modification 5
 - 2.2 Related Work: Quality Assessment Metrics 7
 - 2.2.1 Overview 7
 - 2.2.2 Object Space Approaches 8
 - 2.2.3 Image Space Approaches 13
 - 2.3 Background: Human Visual System 17
 - 2.3.1 Spatial Frequency Sensitivity 18
 - 2.3.2 Bandpass Filters 21
 - 2.3.3 Temporal Adjustments 23

- 3 The System** **27**
 - 3.1 Overview 27
 - 3.2 Spatial Frequency Sensitivity 28

3.2.1	Curvature Computation	31
3.2.2	Weighted Curvature Variance Computation	32
3.2.3	3D Spatial Frequency Sensitivity Function	34
3.3	Visual Selectivity Model	36
3.4	Temporal Adaptations	38
4	Evaluation	40
4.1	Experimental Design	40
4.1.1	User Test Procedure	41
4.1.2	Setup	42
4.1.3	Subjects	43
4.1.4	Data	43
4.2	Results & Analysis	44
5	Conclusion	49

List of Figures

2.1	A mesh (leftmost) and two levels of simplification results using a popular mesh modification library (CGAL)	6
2.2	Smoothed mesh models for noise reduction or reducing artifacts	7
2.3	Root Mean Squared Distance of a vertex pair of mesh M_A and M_B . The average of vertex pair distances give mesh distance value.	8
2.4	Hausdorff algorithm visualization. For each vertex of mesh M_A minimum distance to vertices of mesh M_B is computed. Distance between M_A and M_B is the maximum of the pair-wise minimum distance	9
2.5	Mean curvature estimation of a mesh calculated by [28]	10
2.6	An example distance map between two images for luminance and color channels summation	13
2.7	Prediction of detection map by Visual Differences Predictor by [6].	15
2.8	Chromatic and Achromatic Contrast and Frequency Images	16
2.9	Sample stimuli and the luminance oscillation profiles	18

2.10 Pelli-Robson chart. This image has spatial frequency decreasing from right to left and grating contrasts increasing from top to bottom. When viewed from a distance there appears to be a distinct silhouette of the grating and the uni-colored portion. This silhouette indicates our relative sensitivity to different spatial frequencies. 19

2.11 Blakemore’s frequency sensitivity graph for gratings of varying bar width previous before adaptation 20

2.12 (a) Adaptation grating and test gratings (b) Sensitivity function graph after adaptation to grating of 7 cyc deg. The continuous line gives the sensitivity before adaptation. The line is fitted to Figure 2.11’s data. 21

2.13 Cortex filter formation from frequency and orientation varying filters [6]. Difference of Mesa(DOM) filters represent frequency tuning cortex cells and fan filters represent orientation tuning cortex cells. Cortex filters are formed by multiplication of the DOM and fan filters. 22

2.14 (a) Cross-section of adjacent mesa filters and subtraction of them. (b) 2D DOM filters with computed as differences of mesa filter Eq.2.13 [36]. 23

2.15 Cortex filters generated by multiplication of each DOM and fan filter pair [6] 24

2.16 An example flicker (temporal frequency) used in measuring temporal sensitivity 24

2.17 Temporal Contrast Function from Kelly’s [18] temporal adaptation data. 25

2.18	Smooth pursuit compensation and eye tracking velocity graph, from data [7]. Subjects eye's velocity while tracking a target is shown as open circles. The actual velocity is in horizontal axis and the tracking velocities are shown in vertical axis. Solid represents the Daly's heuristic for eye's tracking ability.	26
3.1	Overview of system architecture	28
3.2	An example point v on a surface and its main components	29
3.3	Visualization of spatial frequency and curvature relationship through different grating sine waves	30
3.4	Voronoi region around a point x_i on a triangular surface	32
3.5	A local neighborhood of vertex	34
3.6	Typical Normalized CSF model used by our proposed method	36
3.7	Output sensitivity map of a horse model	36
3.8	A set of mesa filter generated with given equation 3.8	37
3.9	Selectivity map after DOM filter locally application to each vertex	37
4.1	Experimental setup for viewing stage and marking stages	42
4.2	Horse mesh quality assessment experiment: Sample viewer evaluations, difference map and visual comparison of reference and test mesh is given	45
4.3	Hand mesh quality assessment experiment: Sample viewer evaluations, difference map and visual comparison of reference and test mesh is given	46
4.4	Correlation map for all samples combined	47

4.5	Correlation map for each modified mesh of <i>Doll</i> is given.	47
4.6	Correlation map for each modified mesh of <i>Hand</i> is given.	48
4.7	Correlation map for each modified mesh of <i>Horse</i> is given.	48

List of Tables

4.1	Statistics of modified meshes; vertex count, mean edge length and mean face distortions	43
-----	---	----

Chapter 1

Introduction

Problem Definition

The fast developing computer graphics field enables commercial applications widely to use 3D models which can be animated. A large number of these applications rely on manipulation or transmission of the 3D content to function in real time. Therefore, a trade-off arises among visual quality and processing time. To reduce the processing time, numerous modification algorithms on 3D models are used serving purposes such as smoothing, simplification or compression the original content. The final quality of a modification method is dependent on the resulting models visual accuracy with respect to their original model.

In our context, quality assessment in 3D models is a problem of evaluation of a modified mesh with respect to its original form based on detectability of changes. Quality metrics are typically given two slightly different models and compute geometric differences to reach a quality value.

Human visual system (HVS) enables humans to detect robustly the artifacts and differences in 3D models such as triangular spikes, over-smoothed regions, variations in roughness and structural distortions. In contrast, HVS has weaknesses such as masking effect which prevents detection of artifacts. Unfortunately a unified HVS model does not exist which easily and accurately predict the seeing

experience. However there are several HVS models which serve to mimic sub-processes of human visual system. One important group of sub-processes is the seeing after-effects that partially serve to detect differences and distortions. In our proposed model, we have integrated these subprocesses to mimic perceptual aspects of the quality assessment.

Motivation

The existing quality assessment methods do not reflect both the characteristics of the visual system and effect of the 3D nature of the scene. The reason is that, these methods rely only on either computing a 3D geometric distance without considering human visual system or base their metric on HVS and disregard geometric attributes. [?]

HVS models, which are concerned with sensitivity to change in scenes, are formed by visual psychophysical experiments which typically take place in experiment setups specifically for retinal images. These experiments present data in image space and serve effectively in image or video quality evaluation or estimation of 2D imagery artifact detection. HVS models account for contrast sensitivity function for both spatial and temporal frequencies and in addition the effect of visual masking can be drawn from the psychophysical experiments. Since our concern is assessment of perceived quality in 3D models, object-space solution is needed without disregarding the effect of perception. Our proposed metric estimates spatial and temporal characteristics after rendering based on geometric attributes of 3D models and uses them to compute quality map of the modified mesh.

Challenges & Contributions

Comprehending the relation between the perception of differences and 3D geometric structure is an important research area which is interdependent on a wide range of fields including computer graphics, cognitive science and psychophysical research. Thus, developing a quality metric which takes both geometric attributes and human visual system models into account is not an easy task.

Considering that there is not a unified HVS model to identify differences in two retinal images, human visual system is not fully understood. There exist several human visual system models acquired from psychophysical experiments which serve for different purposes. The first challenge is to understand the principles of human visual system and HVS models to use a proper set of models and serve our purpose.

The 3D geometric structure of a mesh and velocity of its parts have significant impact on the rendered image characteristics. Among these characteristics frequency map of rendered images, which in effect form our quality perception, highly depend on geometric structure. Thus, the necessity to create a method for converting 3D geometric attributes to spatial frequency is essential for the accuracy of the quality metrics we are to develop.

The contributions of this thesis can be summarized as follows:

- An object-space quality metric based on Human Visual System models to fully reflect the perceived distances to be used in applications that require a trade-off between processing time and visual quality.
- A new 3D projection method from geometric attributes of the mesh to spatial frequency.
- A visual selectivity method on 3D spatial frequency estimation.
- An evaluation of the developed system with subjective evaluation techniques to reflect its feasibility.

Outline of the Thesis

This chapter served as an introduction to the topic and further chapters gives details on our method.

- Chapter 2 explains sub-processes of the HVS model to serve as a background. In addition, related work on quality metrics of 2D and 3D media is given and a brief survey on modification algorithms is explained.

- In chapter 3, we explain our proposed object-space solution to quality assessment and evaluation problem in detail.
- Chapter 4 gives detailed information on the method of evaluation of the our system and analysis of the results.
- Discussion of the overall method is given in Chapter 5.

Chapter 2

Related Work & Background

2.1 Related Work: Mesh Modification

The range of uses and the demand of the market force a widespread use of 3D graphical elements in applications. The main media in these applications is animated 3D meshes represented by vertices, edges and faces. In addition these applications frequently require changes in the topology of the mesh.

Simplification

To create a visually realistic looking scene a large number of vertices and usually millions of polygons are needed to form detailed models. In contrast, the time it takes to process these huge meshes gets longer. These processes include transmission over a network, storage and indexing, computation and display of these meshes. As a solution to above problems, simplification methods have been developed which reduce the number of polygons and vertices while trying not to lose its geometric form. There are a large number of simplification methods which differ by their use in applications or type of input meshes.

One of the most common simplification algorithms is proposed by Rossignac & Borrel [33]. The algorithm works on triangulated meshes by subdividing the



Figure 2.1: A mesh (leftmost) and two levels of simplification results using a popular mesh modification library (CGAL)

volume into a uniform grid. A single vertex point is computed for each of the grid cells and these vertices are later connected. Low et al. propose a clustering algorithm where the space is divided into cluster cells providing more accurate result and improved the weighting criteria [25]. Guéziec et al. propose a method based on edge collapsing for manifold meshes [13]. Furthermore this work is extended by Garland et al. to be used for non-manifold meshes [10]. They proposed a method for vertex collapsing, where two vertices are not required to be connected by an edge to be collapsed. Example simplification method applied on a mesh and its results are shown in Figure 2.1

Smoothing

In the process of generation of 3D meshes, artifacts or noise can be present. Smoothing is a post-process method to increase the mesh quality where vertex locations are adjusted while preserving the vertex count and connectivity. There are many smoothing algorithms presented. The most common of them is Laplacian smoothing which repositions a vertex by averaging the neighboring vertex coordinates [16]. This approach is extended to handle non-regular grids by equalizing volume of vertices to adjust. [34]. Knupp et al. present the elliptic smoothing to work on unstructured and structured meshes [20]. Brewer et al. propose another approach by moving interior vertices in order to optimize the mean ratio [3]. An example smoothing algorithm applied on “Stanford bunny” mesh is shown in

Figure 2.2

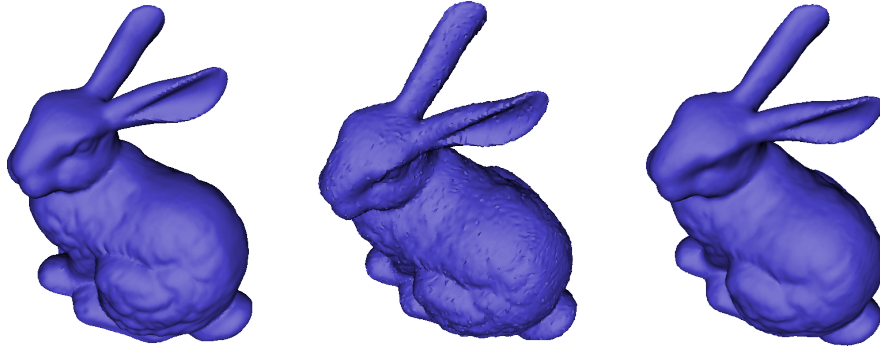


Figure 2.2: Smoothed mesh models for noise reduction or reducing artifacts

2.2 Related Work: Quality Assessment Metrics

2.2.1 Overview

Quality assessment metrics aim to estimate a similarity between a given mesh and its modified version. An original mesh can be modified by simplification, smoothing, etc. As the quality assessment methods are comprehensively studied, there exists a wide range of proposed solution criteria.

Existing quality metrics can be divided into two types as *object-space* and *image-space* approaches. Image space based methods typically use a pre-rendered 2D image to compute a quality value whereas object-space approaches operate on the 3D mesh. This distinction significantly effects the output of the methods since environment conditions such as lighting position, lighting strength, viewing angle have great impact on the rendered image. 3D models' quality should not depend on these highly varying states.

This section will cover the range of existing methods to that are being used to measure similarity between two meshes.

2.2.2 Object Space Approaches

2.2.2.1 Mathematical Difference Measurements

Geometric distance between two objects is commonly used for geometric computations such as collision detection and motion planning. Fast and efficient algorithms are developed to suit such needs.

The simplest and most pure mathematical difference between two meshes is the root mean square computation:

$$RMS(M_A, M_B) = \sqrt{\sum_{i=1}^n \|v_{ai} - v_{bi}\|^2} \quad (2.1)$$

where M_A and M_B are two meshes. $v_{a1} \dots v_{an}$ and $v_{b1} \dots v_{bn}$ are vertices of M_A and M_B respectively. Euclidean distance between two vertices v_i and v_j is denoted by $\|v_i - v_j\|$. RMS measure requires two meshes to have the same number of vertices and the same connectivity. RMS is not preferred for most quality assessment methods since the resulting values do not represent visual characteristics.

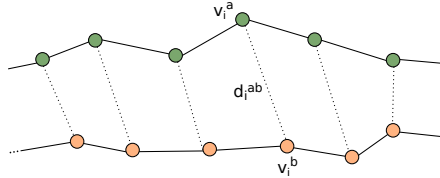


Figure 2.3: Root Mean Squared Distance of a vertex pair of mesh M_A and M_B . The average of vertex pair distances give mesh distance value.

Hausdorff distance is a common metric for comparing two meshes. Hausdorff distance is the maximum distance of a set to the nearest point of another set, where a set contains only vertices. The distance of M_A to M_B is given by:

$$h(M_A, M_B) = \max_{v_{ai} \in M_A} (\min_{v_{bi} \in M_B} (d(v_{ai}, v_{bi}))) \quad (2.2)$$

$$d(v_i - v_j) = \|v_i - v_j\| \quad (2.3)$$

Here, the distance between vertices is denoted as $d(v_i, v_j)$ is the Euclidean distance between vertices v_i and v_j .

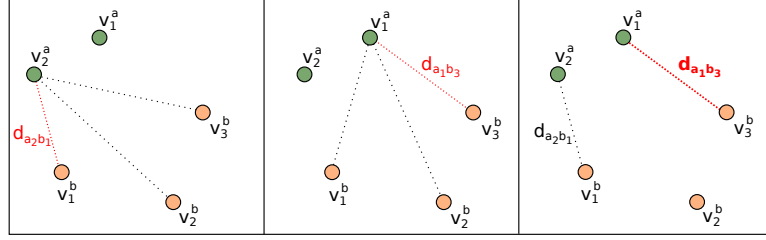


Figure 2.4: Hausdorff algorithm visualization. For each vertex of mesh M_A minimum distance to vertices of mesh M_B is computed. Distance between M_A and M_B is the maximum of the pair-wise minimum distance

Note that this Hausdorff distance definition is asymmetric [4] and is called “one-sided Hausdorff distance”. The two-sided Hausdorff distance between two meshes is the maximum of the one-sided Hausdorff distances of the meshes to each other:

$$H(M_A, M_B) = \max(h(M_A, M_B), h(M_B, M_A)) \quad (2.4)$$

The algorithm for the brute force solution of Hausdorff distance is given as:

Algorithm 1 Hausdorff Distance

```

h ← 0
for all vi ∈ V(MA) do
  shortest ← Inf
  for all vj ∈ V(MB) do
    dij = d(vi, vj)
    if dij < shortest then
      shortest ← dij
    end if
  end for
  if shortest > h then
    h ← shortest
  end if
end for

```

2.2.2.2 Curvature Based Measurements

A mesh’s shape is formed by different types of surface patches such as smooth, rough or edge regions. Types of surface patches influence our sensitivity to changes.

For instance, subtle changes are prone to be seen when occurring in smooth regions rather than rough regions. Therefore, determining the structural characteristic of the mesh is important for quality assessment methods. Curvature of vertices indicates roughness and structure therefore existing quality measurement methods integrated curvature attribute in their solutions.



Figure 2.5: Mean curvature estimation of a mesh calculated by [28]

Karni used a Laplacian operator in addition to simple geometric distance to reflect visual difference better in their mesh compression algorithm [17]. The Laplacian operator takes into account the geometry and topology and the geometric Laplacian at vertex v_i is:

$$GL(v_i) = v_i - \frac{\sum_{v_j \in n(v_i)} d(v_i, v_j)^{-1} v_j}{\sum_{v_j \in n(v_i)} d(v_i, v_j)^{-1}} \quad (2.5)$$

where $d(v_i, v_j)$ is the geometric distance between vertices i and j , and $n(v_i)$ is the set of neighboring vertices of v_i .

In order to incorporate the above geometric Laplacian, the average of the norm of the Laplacian distance and the norm of the geometric difference is taken as the resulting difference between two meshes.

$$d(M_A, M_B) = \frac{1}{2n} (d(v_{ai}, v_{bi}) + d(GL(v_{ai}), GL(v_{bi}))) \quad (2.6)$$

The above geometric Laplacian operator (eq 2.5) gives the geometric difference between the original coordinates of the vertex v_i and its position after Laplacian

smoothed. This results in a form of roughness measurement and gives accurate results on compressed meshes.

In addition, roughness variation has been used as a heuristic to quality preservation in mesh simplification schemes. Wu et al. [38] used roughness of a vertex neighborhood to preserve high-frequency details. Their simplification scheme uses variances in dihedral angles between triangles to reflect local roughness and weigh mean dihedral angles according to the variance. $G(t)$ is calculated for each face of the mesh. Given a triangle t , $G(t)$ is the weighted sum of average dihedral angles of the neighboring triangles:

$$G(t) = \frac{G_1 \cdot VAR_1 + G_2 \cdot VAR_2 + G_3 \cdot VAR_3}{VAR_1 + VAR_2 + VAR_3} \quad (2.7)$$

$G_{1,2,3}$ and $VAR_{1,2,3}$ are mean dihedral angles and variances for each triangle vertex. Assume that n number of triangles share the vertex of v_1 of t . To calculate $G(t)$, $n - 1$ number of dihedral angles between $t - t_1$, $t_1 - t_2$, \dots , $t_{n-1} - t$ are computed which are then used to compute G_1 and VAR_1 . Similar computation is conducted for v_2 and v_3 .

Roughness of a 3D mesh has been also used to measure quality of watermarked meshes [11] [5]. Drelie Gelasca et al. used roughness to evaluate the difference between a given mesh and its watermarked version. In their work roughness is computed for each vertex by calculating the variances in distances of local vertices:

$$r(v) = \frac{\sum d(v, v_i)}{A_v} \quad (2.8)$$

where v_i is in a pre-defined radius and A_v is the total area of the faces for a given radius. Later, roughness of a mesh is computed by summing up the roughness values of all vertices. The difference between the original mesh and the watermarked mesh is given by the formula:

$$R(M_A, M_B) = \log \left(\frac{R(M_A) - R(M_B)}{R(M_A)} + k \right) - \log(k) \quad (2.9)$$

where M_A and M_B denote the original and watermarked meshes respectively.

Curvature has also been used to represent structure of a given mesh. Quality assessment through mesh structure is studied by Lavoué et al [21]. The method

computes mesh's roughness using a 3D window definition. Then a visual evaluation of the masking effect and its relation to proposed roughness measure is conducted.

2.2.2.3 Attribute Based Measurements

3D Meshes typically have non-geometric attributes such as texture, color and material properties. The appearance of the mesh is controlled by these attributes. Distortion or defects caused by errors in these attribute values are detected easily by the human visual system, thus reducing the quality.

Several studies draw attention to this property of 3D meshes [27] [29]. Luebke et al. focus on difference measurement and point that the Hausdorff distance does not handle the geometric distance with respect to such attributes [27]. This study proposed an alternative distance measurement called bijection distance measurement. Bijection requires a continuous, one to one mapping between attributes of the meshes at each vertex and the relative distance between them regarding the mapping.

Another important study bases the quality to be related to texture and wireframe [29]. This study aims to determine the importance of texture and wireframe resolutions with respect to each other. In addition, a quantitative evaluation strategy is proposed for 3D quality.

$$\mathcal{Q}(g, t) = \frac{1}{\frac{1}{m+(M-m)t} + \left(\frac{1}{m} - \frac{1}{m+(M-m)t}\right) (1-g)^c} \quad (2.10)$$

Here, g and t are graphical and texture components scaled into $[0 \dots 1]$ interval, m and M are the minimum and maximum bounds of quality, and c is a constant. All constants and coefficients are determined by experimental data.

2.2.2.4 Saliency Contribution

Saliency is studied in many visual and graphics fields and 3D mesh geometric characteristics plays an important role when determining saliency. Several quality

assessments methods are purely based on weighting geometric distance based salient regions of the mesh. Mesh simplification methods integrate saliency to the algorithm to preserve saliency parts of meshes. Studies by Howlett et al. [14] and Lee et al. [22] focus on saliency effects on mesh simplification.

2.2.3 Image Space Approaches

2.2.3.1 Mathematical Difference

Mathematical difference computation of single images or sequence of images has been sought as a quality assessment method. These methods rely only on Euclidean distances between corresponding pixels on images in color space and determine a quality value or a reach a difference map between two sets Figure 2.6.

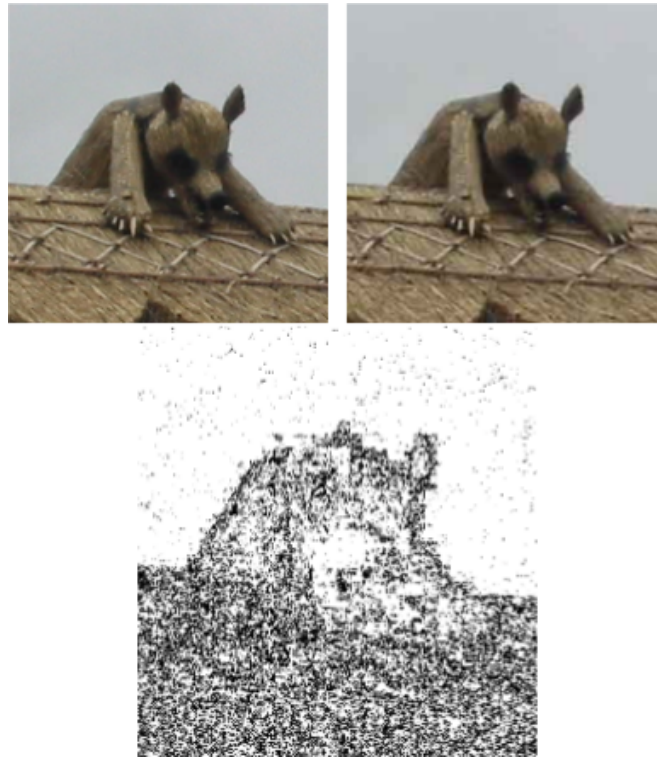


Figure 2.6: An example distance map between two images for luminance and color channels summation

In their study, Turk et al. used root mean squared (RMS) as image error

for 3D mesh simplification. The quality of the mesh is determined by taking several viewpoints, rendering the original and the simplified mesh from the same viewpoints and calculated the RMS between two images. The distance between two images is given by:

$$d_{RMS}(Y^0, Y^1) = \sqrt{\frac{1}{mn} \sum_{i=1}^m \sum_{j=1}^n (y_{ij}^0 - y_{ij}^1)^2} \quad (2.11)$$

This measure does not take into account human visual system and does not give accurate results. Therefore it is seldom used as a perceptual quality metric for 3D meshes.

Peak signal-to-noise ratio (PSNR) is a method that is widely used to estimate the difference and error between two images. This quality metric calculates the PSNR of an image against its reference image. Using root mean squared (RMS) error in Eq. 2.11, PSNR is calculated as:

$$PSNR = 20 \log_{10} \left(\frac{I_{max}}{d_{RMS}} \right) \quad (2.12)$$

where I_{max} is the maximum possible pixel luminance value. This metric gives good error indications for images of natural spaces. In contrast, this measure is not a good metric for images of human-made objects and places. [35]

2.2.3.2 Visual Sensitivity Measurements

Psychophysical experiments operate on 2D image and are concerned with retinal images which are in image space. Therefore, quality measurement or estimation methods working on image space solutions are able to take full advantage of HVS models.

Most used and known of image-based measurement methods is “Visible Differences Predictor (VDP) ” proposed by Daly [6]. VDP algorithm describes the human visual system response by image-processing approach. Preserving the phase information is crucial in VDP algorithm for calculation of masking effects. HVS response to the image is relative value of a test image with respect to a reference image, rather than an absolute value of a single image. The value of

quality or probability of detection is not collapsed to a single value as in other image-quality methods. Instead, the value is preserved as a 2D “probability of detection” map. An example quality difference map is shown in Figure 2.7

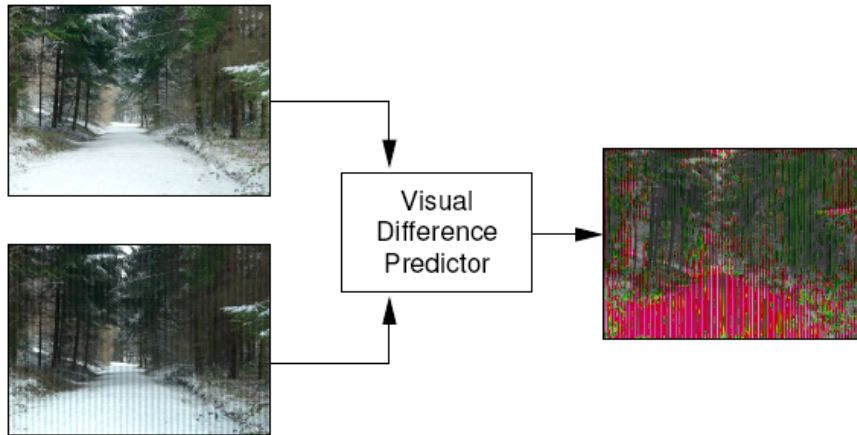


Figure 2.7: Prediction of detection map by Visual Differences Predictor by [6].

Longhurst et al. measured the fidelity of VDP method [24]. In their psychophysical experiment, they have measured the correlation between the methods’ prediction and the subjective evaluations of the users.

A similar quality metric is Sarnoff Visual Discrimination Model (Sarnoff VDM) proposed by Lubin [26]. Sarnoff VDM is aimed for fast and accurate distortion prediction on large number of image quality rating tasks. VDM also produces a probability of detection map. Li et al. compared VDP and Sarnoff VDM with their own implementation of the algorithms [23]. Analysis of the two algorithms showed that the VDP takes place in feature space and takes advantage of FFT algorithms but lack of evidence of these feature space transformations in HVS gives VDM an advantage. Also FFT takes most of the processing time during VDP algorithm.

Bolin and Meyer based their vision model on Sarnoff VDM with reduced processing time and addition of color adaptations [2]. Chromatic and Achromatic contrast sensitivity functions Figure 2.8 were used for color extension to the VDM model. Bolin and Meyer’s (BM) solution models the early human vision stages. They have used this new vision model for their global illumination algorithm.

Fidelity of the proposed method is measured, and naming time and quality difference was the most reliable among other methods [37]. It is also noted that Bolin & Meyer’s method is a ”severe simplification“ of human visual system.

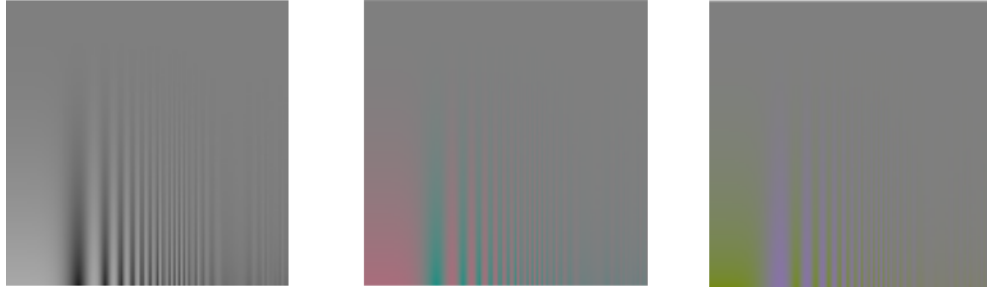


Figure 2.8: Chromatic and Achromatic Contrast and Frequency Images

Ramasubramanian et al. [31] introduced a error detection metric that handles luminance and spatial processing independently. Pre-processing spatial components increases efficiency of the algorithm. The study incorporates the proposed perceptual model to their global illumination method for image synthesis.

A framework measuring visual equivalence is proposed by Ramanarayanan et al. [30] (VEP). Visual impressions of scene appearance is analyzed and the method output a visual equivalence map. Geometry, material and illumination effects on visual impressions are studied by conducted experiments. The output maps of the method can indicate visual equivalence even the regions are visibly different because of visual impressions phenomena. The study focuses on two types of transformation of illumination; blurring and wrapping. Lastly, their study presents examples of how VEP can be used to improve existing modification algorithms.

An extension of these image-space solutions to applications in 3D is examined by Ferwerda et al. [9]. The study showed relationship between mesh structure and contrast masking. Effects of masking are shown by example where one visual pattern (texture) masks another pattern (contrast due to structural distortions). The study also computed VDP values of textures and gave visual examples how VDP values can be used to relate to masking effects. In a similar point of view Lavoué [21] measured 3D roughness values of mesh and linked roughness to visual masking. Relationship between roughness values and masking effects were shown

by visual examples and 3D computation of the work is solely considered object-space. Both these studies focuses on masking effects on 3D surfaces but did not extend their method to link 3D structure to the HVS viewing models.

2.3 Background: Human Visual System

Perceptual Computer Graphics has drawn attention from researchers due to the fact that what is perceived is as significant as what is displayed on the screen. Studies showed that generation, evaluation and usage of graphics can take advantage of human visual system's characteristics. Therefore, understanding human visual system is essential for perception-based computer graphics research.

Human visual system is a complex mechanism and has not been fully understood by psychophysics researchers. Human visual system handles a wide-range of tasks such as object-recognition to motion, color and depth perception. Each of these tasks are accomplished by going through human visual system sub-processes. For example, object recognition is accomplished by cortex cell's adaptations for edge detection, figure from background and matching alignment and stored objects. Similarly, difference detection goes through several sub-processes.

The three psychophysical concepts affecting sensitivity to changes are:

- Spatial Frequency Sensitivity
- Bandpass Filters
- Temporal Adjustments

All three sub-processes are categorized as aftereffects of seeing. These are neurological phenomena which appear for constant stimuli. It is known that such effects occur widely in sensory systems. Following subsections explain these phenomena and explain computational approaches to them.

2.3.1 Spatial Frequency Sensitivity

Intensity values across two dimensional space construct spatial features of an image. The sensitivity to change in spatial features has been experimentally studied starting from late 1960s [1]. Studies focusing on this phenomena measure the response of the observer to varying parameters; contrast, frequency, orientation and phase.

Psychophysical experiments measuring HVS responses to spatial frequency use grating of sine waves (sinusoid) that appear as a stimuli. Psychophysical experiments measure the spatial frequency in cycle per degree (in visual angle metric). The wave is described as frequency for its oscillation between high and low luminance levels Figure 2.9. The metric is defined where 1° visual angle is described as 1 cm portion of image viewed at 57.3cm distance.

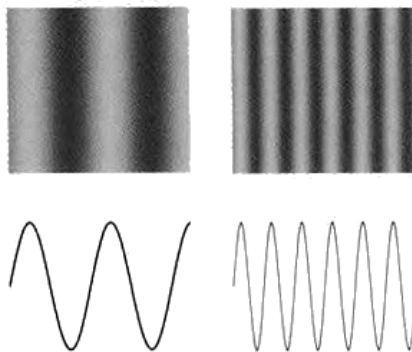


Figure 2.9: Sample stimuli and the luminance oscillation profiles

The spatial frequency experiments are in a test-adapt-test manner, where the subjects are first tested without adaptation and later tested for adaptation to a stimuli. Appendix gives a sample experiment setup for spatial frequency tests and experience the difference detection mechanisms.

The stimuli to these experimental studies are typically luminance gratings. These gratings are laboratory stimulus with strips of light and dark bars with varying contrast and frequency. In these gratings, sine wave is used as the pattern to strips. Below is Pelli-Robson chart where frequency detection is experienced as

an aftereffect.

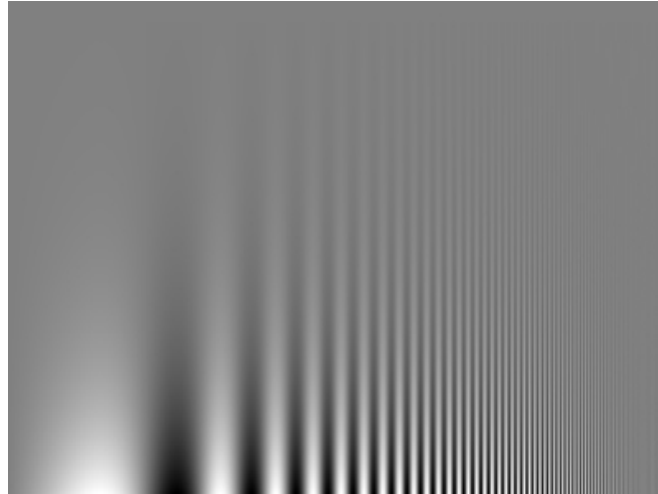


Figure 2.10: Pelli-Robson chart. This image has spatial frequency decreasing from right to left and grating contrasts increasing from top to bottom. When viewed from a distance there appears to be a distinct silhouette of the grating and the uni-colored portion. This silhouette indicates our relative sensitivity to different spatial frequencies.

The experiment input stimuli vary in four parameters:

- Frequency: the number of cycles per degree of visual angle. The spatial frequency depends on viewing distance because the grating that falls into one degree changes.
- Contrast: the brightness or the darkness of the object with respect to its neighborhood (field of view).
- Orientation: the tilt angle of the stripes in clockwise direction. The origin orientation is taken to be vertical tilt.
- Phase: the alignment of a fixed reference with the grating cycle.

The classical and basic experiment results by Blakemore et al. [1] are given in Figure 2.11. The data obtained from the experiment is measured without adaptation effects.

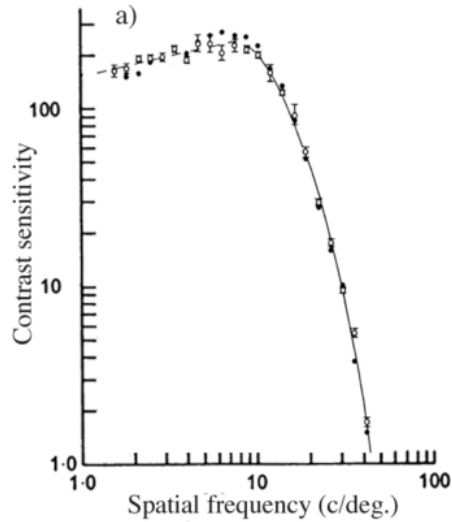


Figure 2.11: Blakemore's frequency sensitivity graph for gratings of varying bar width previous before adaptation

This CSF given by Blakemore et al. [1] shows detection of a change luminance depends on both frequency and contrast. Spatial frequency sensitivity starts to decrease after 10 cpd and significantly drops after 20-30 cpd. Frequencies higher than 40 cpd are undetectable even with higher contrast values. Also, gratings with 1.0 cpd have lower sensitivities than 10 cpd and sensitivity to change in luminance gradually increases from 1.0 cpd to 10 cpd.

Effect of Adaptation

Further experiments measuring the effects of adaptation to a fixed cycle per degree are conducted. The resulting responses are given in Figure 2.12. The results show an obvious decrease in sensitivity post-adaptation experiment results. The black squares represent mean subject responses and the adaptation frequency in the experiment is 7 cpd. The drop obviously occurs around selected adaptation spatial frequency. This is interpreted as more contrast is needed to be seen at the same grating. The adaptation experiment indicates that there is a set of channels, each one tuned for a narrow range of spatial frequencies. Next subsection explains tuning in detail.

The tuning of each channel can be measured neuro-physiologically by using microelectrodes to measure the responses of neurons to gratings of different spatial

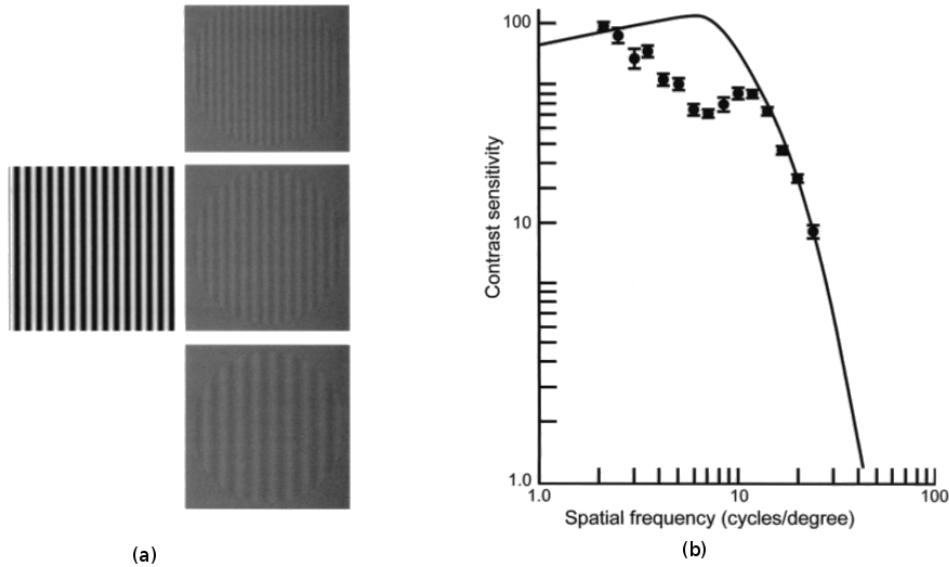


Figure 2.12: (a) Adaptation grating and test gratings (b) Sensitivity function graph after adaptation to grating of 7 cyc/deg. The continuous line gives the sensitivity before adaptation. The line is fitted to Figure 2.11's data.

frequencies.

2.3.2 Bandpass Filters

Adaptation experiments reflect responses of tuning mechanisms to spatial frequency. Mathematical analysis of these tuning mechanisms results in computationally derived bandpass filters or equivalently channels. Further experiments on orientation result in a similar tuning for oriented gratings. Therefore, computational HVS models generate internal representation composed of channel responses where each channel has an orientation and frequency tuning.

The tuning to frequency and orientation is limited to a certain cycle per degree and orientation giving rise to gabor filter representations of images. Cortex transformation is another important model for frequency and orientation selectivity proposed by Watson [36]. Frequency tuning is modeled by difference of mesa filters and orientation tuning is modeled by fan filters, as shown in Figure 2.13. Cortex transform of an image is computed by using steps:

1. Transform: Cortex transformation filters are applied to the image
2. Quantize: Reduction to finite numbers of the filters
3. Reconstruct: Cortex response of the cells are computed.

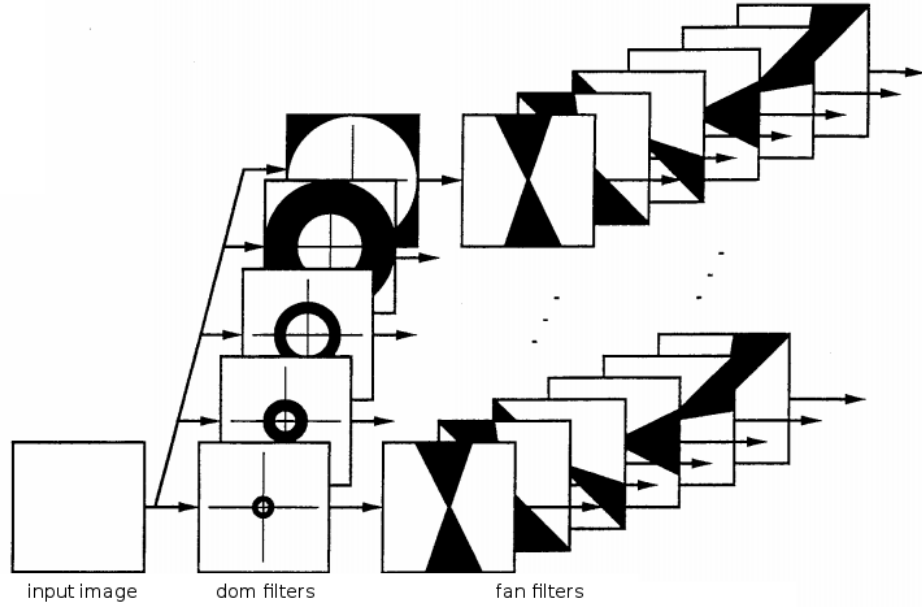


Figure 2.13: Cortex filter formation from frequency and orientation varying filters [6]. Difference of Mesa(DOM) filters represent frequency tuning cortex cells and fan filters represent orientation tuning cortex cells. Cortex filters are formed by multiplication of the DOM and fan filters.

Below subsections explain the cortex transformation applied to the image.

Frequency Tuning

Frequency tuning is achieved by a set of difference of mesa filter (DOM Filters). Mesa filters are defined as blurry disks in the frequency domain. This filter is formed by Gaussian filtered cylinder and is given by the formula:

$$m(u, v) = \left(\frac{\gamma}{f}\right)^2 \exp\left[-\pi\left(\frac{r\gamma}{f}\right)^2\right] * \Pi\left(\frac{r}{2f}\right) \quad (2.13)$$

where u, v are x, y coordinates and relative to origin, r is the distance to origin. Π is the rectangular response of unit height and width. The Gaussian can be controlled by the γ which is a sharpness parameter. The scale parameter (s) of

the mesa filter can be added by multiplication of u and v values with s . Difference of mesas can be found by subtraction of adjacent mesa filters.

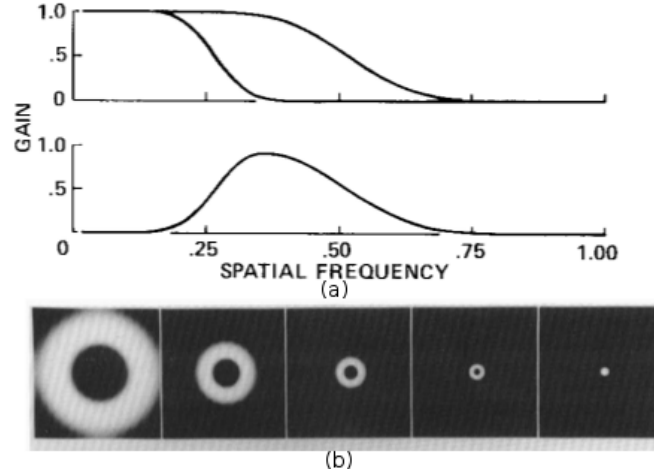


Figure 2.14: (a) Cross-section of adjacent mesa filters and subtraction of them. (b) 2D DOM filters with computed as differences of mesa filter Eq.2.13 [36].

Orientation Tuning

Orientation tuning mechanism is modeled by fan filters which are obtained by bisection of space. Orientation bandwidth can be different degrees. Watson used 45° degrees to form 4 orientations ($\Omega = 4$) [36].

$$f_i = b_{i\delta}(1 - b_{(i+1)\delta}) + b_{(i+\Omega)\delta}(1 - b_{(i+1+\Omega)\delta}) \quad (2.14)$$

where $i = 0, \dots, (\Omega - 1)$.

Cortex Filter

For each one of DOM filters, a fan filter is generated Figure 2.15 Each row forms a frequency and columns form orientation filters.

2.3.3 Temporal Adjustments

Temporal features of an image are differences in intensity across time. The detectability of change in temporal features has been studied starting from late 1950s [8]. One notable study on temporal sensitivity is conducted by Kelly et al. [18]. To measure temporal sensitivity, a simple shape is shown to observers while

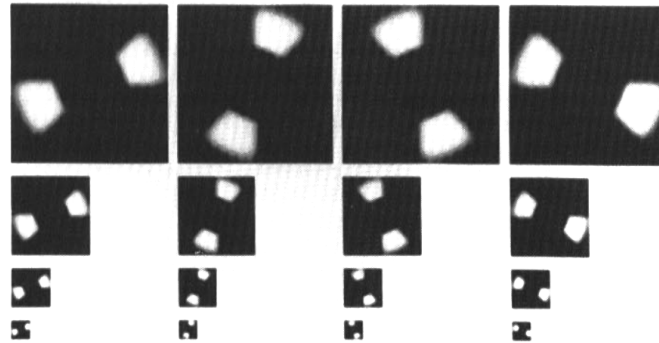


Figure 2.15: Cortex filters generated by multiplication of each DOM and fan filter pair [6]

switching between black and white. This switching behavior is called the flicker and the speed of flicker is "flicker rate" or "temporal frequency". A "cycle" is the change from black to white and black again and the "period" is the time that one cycle takes. The intensity of luminance of the shape changes depending on the contrast.

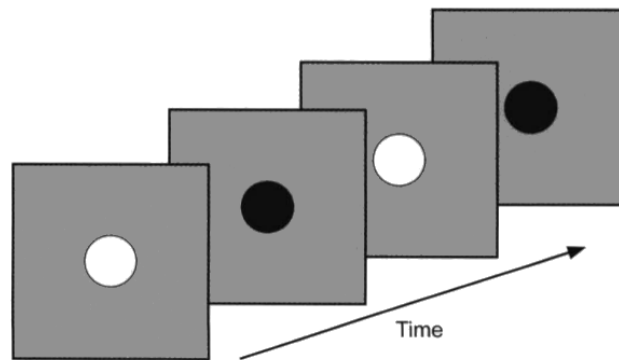


Figure 2.16: An example flicker (temporal frequency) used in measuring temporal sensitivity

The stimulus for temporal sensitivity experiments is a simple shape with alternating luminance, the intensity of luminance is changes with contrast. An example temporal frequency is given in Fig. 2.16. The change of two parameters are tested:

- Contrast: the brightness or the darkness of the object with respect to its

neighborhood (field of view).

- Temporal Frequency: the number of cycles elapsing over 1 sec (Hz). The sequence should be alternating between a darker and a lighter tone of luminance.

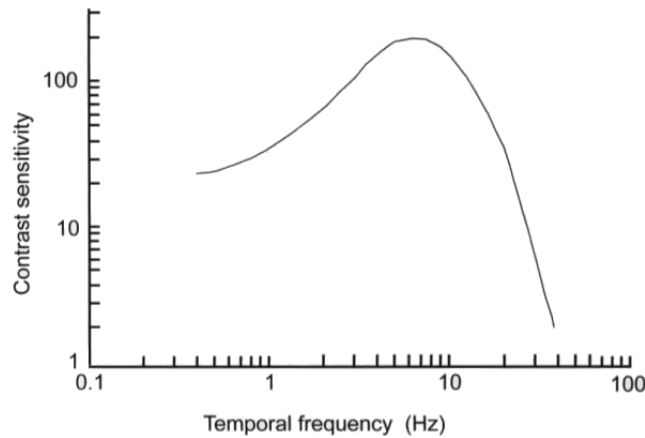


Figure 2.17: Temporal Contrast Function from Kelly’s [18] temporal adaptation data.

The results of this experiment can be plotted in temporal contrast sensitivity function, as can be seen in Figure 2.17. Similar to spatial CSF, the sensitivity depends on both contrast and temporal frequency. The sensitivity is at its highest value around 8 Hz and decreases rapidly on both directions. After 50 Hz the change in luminance is undetectable even with higher contrasts.

Eye Movements Adaptations

The sensitivity decrease to high temporal frequency stimulus enables to expand existing HVS models. In addition to temporal frequency sensitivity, the eye’s tracking ability is another important factor. This phenomena is known by eye’s ability to track objects of interest where salient parts is higher than the remaining scene. This ability compensates for the loss of sensitivity due to motion. Eye’s tracking ability is also known as *Smooth Pursuit*.

The eye can track objects with speeds up to 80 deg/sec. Until that point, smooth pursuit reduces the speed of object in interest to a certain degree. There

are experiments to measure the compensation and draw a heuristic. The result of measurements by Daly is shown in Figure 2.18.

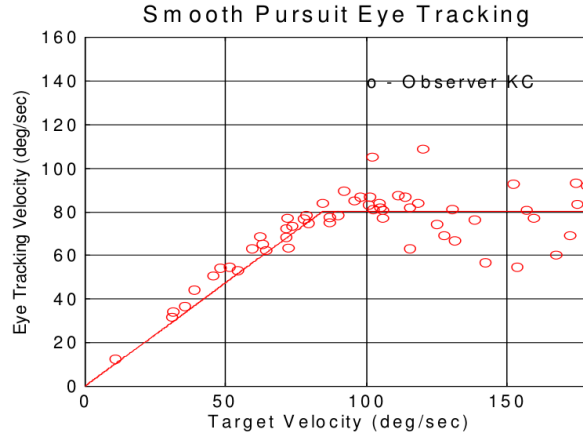


Figure 2.18: Smooth pursuit compensation and eye tracking velocity graph, from data [7]. Subjects eye's velocity while tracking a target is shown as open circles. The actual velocity is in horizontal axis and the tracking velocities are shown in vertical axis. Solid represents the Daly's heuristic for eye's tracking ability.

According to the results of the experiment, Daly introduced a heuristic for smooth pursuit. The equation of the heuristic is:

$$v_R = v_I - \min(0.82v_I + v_{min}, v_{max}) \quad (2.15)$$

where v_R is the retinal velocity, v_I is the actual velocity, v_{min} and v_{max} is drift velocity of the eye and maximum tracking speed respectively.

Chapter 3

The System

3.1 Overview

Our approach presents a quality metric for animated 3D meshes and comprises human visual system models, which based on empirical research on cortex cell adaptations. To compute the quality of a mesh, attributes of a mesh are used, such as geometric placement and temporal change at each vertex. Moreover, in contrast to quality metrics solely using geometric information, when perceptual differences are calculated, human visual system models are needed. Accordingly, our proposed object-space solution integrates an HVS model and has three main stages and uses two animated 3D meshes as input and predicts perceived differences as a 3D map. Integrated HVS prediction method evaluation of a single mesh can also serve as a guide for modification methods or weight factor similar to saliency integrated modification models.

An overview of the system architecture is given in Fig. 3.1. The proposed method starts with calculation of spatial frequency sensitivities. The relation between geometric characteristics impacts the resulting spatial frequency on rendered images. Our method estimates spatial frequency for each vertex by finding mean curvature and a local window definition. To find the sensitivity values, the CSF equation is calibrated to 3D viewing conditions with several

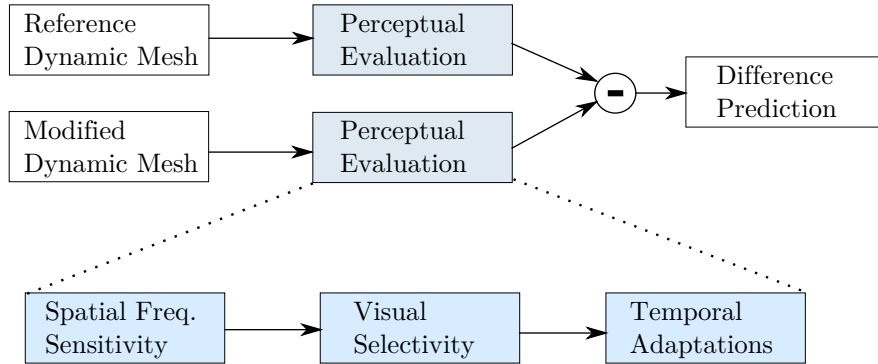


Figure 3.1: Overview of system architecture

assumptions. Later CSF is applied to estimated frequency values at each vertex.

On the second module, the method mimics visual selectivity of the HVS models by use of Difference of Mesa (DOM) filters. Visual selectivity is the HVS adaptation of tuning to narrow ranges of frequency as explained in Section 2.3.2. Filters operate on local neighborhood/window area for each vertex, therefore each vertex sums the neighboring filter effects. Since DOM filter effects are similar to a Gaussian operation, the resulting 3D map at this point is very similar to blurred roughness values on visual inspection.

Temporal adaptations are the last HVS model module in our proposed method. Vertex velocity values are adjusted accordingly to smooth pursuit, eye’s object tracking ability. Temporal sensitivity experiment data is used to weigh the selectivity results in previous step as a last operation. To measure the differences between models, value differences are calculated for each vertex to form a unified 3D prediction of distortion detectability map.

3.2 Spatial Frequency Sensitivity

A computational HVS model uses spatial frequency values to find visual sensitivities. Thus, quality assessment metrics typically expects a 2D image, transforms it into luminance and chromatic channel representations and lastly uses a Gaussian pyramid to compute frequency for that specific image. This approach is suitable

for media that is in image-space, such as videos and pictures. When dealing with 3D media, such as 3D meshes, the above approach is not applicable. Thus, we have adopted a heuristic which evaluates characteristics of 3D meshes effecting spatial frequencies of rendered 3D images.

3D meshes have several attributes contributing to spatial frequency when visualized. Curvature, texture, surface material types and color all contribute to spatial frequency. Curvature has been related to spatial frequency most often as a roughness measure and structure indicator. Previous studies indicate and refer to the relationship between the curvature and spatial frequency. We based our spatial frequency estimator on curvature and studied its effects.

Spatial frequency is peak to peak distance by definition, so our 3D spatial frequency bases curvature calculations on defining a new 3D peak to peak distance value estimation method. Local peaks in 3D are local areas where curvature changes are greater than any smooth patch. Therefore, mean curvature value changes with weight factor as inverse distance gives a 3D peak estimation along with 3D spatial frequency estimation.

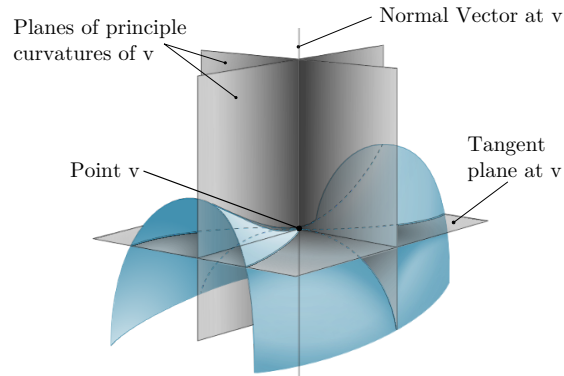


Figure 3.2: An example point v on a surface and its main components

Curvature of a vertex on a 3D mesh is the deviation of that vertex's flatness from neighboring vertices. Components such as normal vector, tangent plane and principle curvatures are computed to reach a curvature value a given point v on a surface as can be seen in Fig 3.2.

Spatial frequency is linked to variance in 3D discrete curvature and studies

have used this curvature as a 3D perceptual measures [19], [22]. To fully capture the relationship between curvatures and frequencies an example is given based on simple sine waves. In Fig. 3.3 visualizations of 2D sine waves which are extended to 3D with varying wavelengths ($\omega = 15, 20, 30$) and amplitudes ($A = 0.2, 0.5$) with phase $\varphi = 0$. Curvatures are calculated with the method which will be explained in detail later.

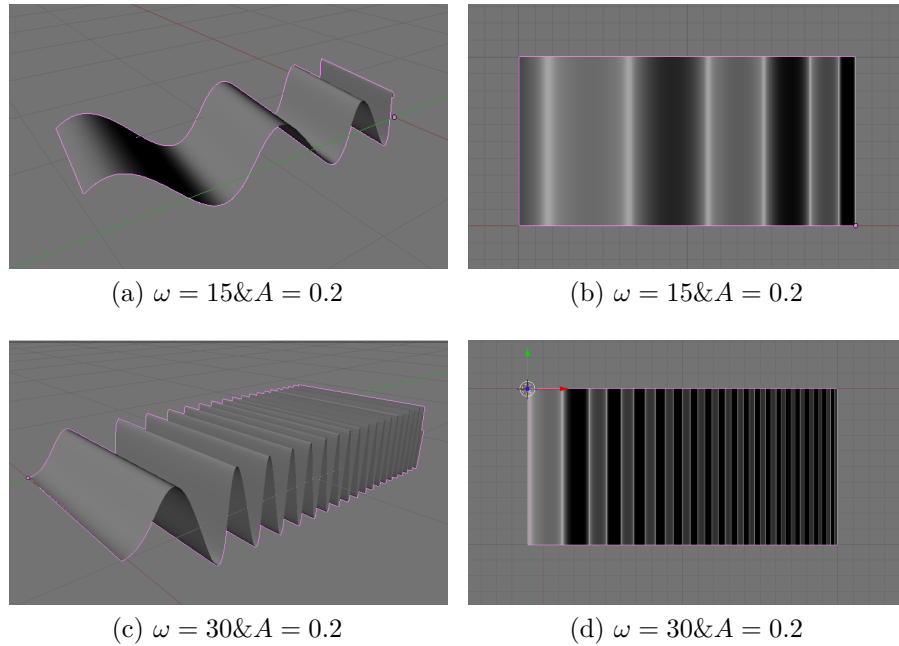


Figure 3.3: Visualization of spatial frequency and curvature relationship through different grating sine waves

Fig. 3.3a and Fig. 3.3b are two views of the same sine wave. Perspective and top views visualize the meshes and present a possible rendering scheme. In Fig. 3.3a curvature is visualized by hue coloring and frequency is expected to decrease slowly with time, as can be seen from the sample rendering (Fig. 3.3b). Latter two images (Fig. 3.3c, 3.3d) show the same sine wave but with different amplitude and wavelength. Here the wavelength decreases greatly with time and it is expected to have greater curvature and spatial frequency. In Fig. 3.3c curvature values are given and as expected curvature values are greater, also from the sample rendering it is obvious that the frequency is higher.

The mapping between curvature and spatial frequency is calculated by finding

weighted curvature variance values for each vertex. This value serves as an estimation of spatial frequency at each specific point on the mesh. Our spatial frequency estimator computes mean curvatures for each vertex of the mesh and weighted curvature variances are computed according to these values. Spatial Frequency Sensitivity functions are later applied to 3D spatial frequency values with adaptations to 3D viewing assumptions.

The algorithm of spatial-frequency estimation is given below:

1. The mean curvature K_i is calculated for each vertex i by using normal vectors and Voronoi area at 1-neighborhood of vertex v_i
2. Weighted variance is calculated for the local window for each vertex.
 - Weight of a neighboring vertex v_j of vertex v_i corresponds to the distance between v_i and v_j 's projection to tangent plane of v_i .
 - The radius of local window is taken to be %2 of cubic bounding box of the mesh.
3. Spatial Frequency Sensitivity Function (SFS) is applied on 3D spatial frequency values with adaptations to 3D viewing environment.

3.2.1 Curvature Computation

Gaussian and mean curvatures represent important local properties of a surface. On an isosurface, curvatures are computed in infinitely small regions with continuous formula:

$$2\kappa_H \mathbf{n} = \lim_{diam(\mathcal{A}) \rightarrow 0} \frac{\nabla \mathcal{A}}{\mathcal{A}} \quad (3.1)$$

where \mathcal{A} represents a small region around a point and $diam(\mathcal{A})$ denotes diameter of the area.

In triangulated surface with voronoi cells, neighboring triangular areas summed to be these infinitely small regions, thus curvature computation is done by discrete equations.

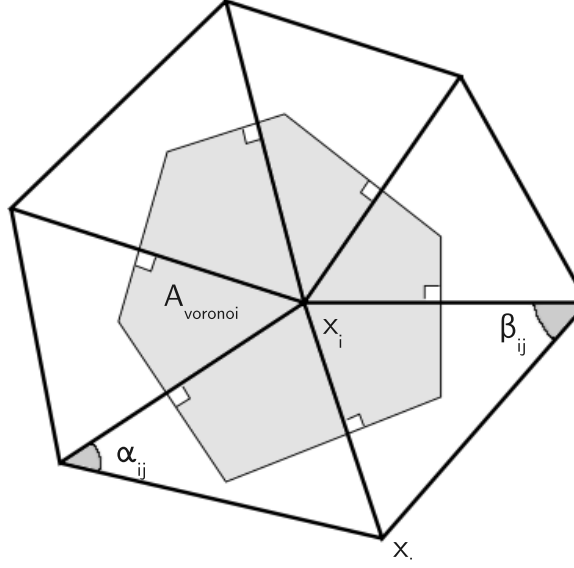


Figure 3.4: Voronoi region around a point x_i on a triangular surface

In Fig. 3.4, a vertex x_i and one of its neighboring vertices x_j is shown. Voronoi region of x_i is than:

$$\mathcal{A}_{\text{voronoi}} = \frac{1}{8} \sum_{j \in N_1(i)} (\cot(\alpha_{ij}) + \cot(\beta_{ij})) \|\mathbf{x}_i - \mathbf{x}_j\|^2 \quad (3.2)$$

where x_j is a direct neighbor of x_i , α_{ij} and β_{ij} is the angles looking towards the edge defined by x_i and x_j vertices.

Mean curvature is then calculated by formula and the pseudocode is given in Algorithm 2:

$$\mathbf{K}(\mathbf{x}_i) = \frac{1}{2\mathcal{A}_{\text{voronoi}}} \sum_{j \in N_1(i)} (\cot(\alpha_j) + \cot(\beta_j))(\mathbf{x}_j - \mathbf{x}_i) \quad (3.3)$$

3.2.2 Weighted Curvature Variance Computation

To estimate the spatial frequency, we use the variance in discrete curvature values in 3D meshes at each vertex. Variance value of a vertex is calculated by using neighboring vertices' curvatures and determining the weight of a neighboring vertex by the distance. The neighborhood of a vertex is local windows with a

Algorithm 2 Calculate Mean Curvature

```

for all  $x_i \in V(S)$  do
   $\mathcal{A}_{x_i} \leftarrow 0$ 
   $K_{x_i} \leftarrow 0$ 
  for all  $x_j \in N_1(x_i)$  do
     $\mathcal{A}_{x_i} \leftarrow \mathcal{A}_{x_i} + (\cot\alpha_{ij} + \cot\beta_{ij})\|\mathbf{x}_i - \mathbf{x}_j\|^2$ 
  end for
  for all  $x_j \in N_1(x_i)$  do
     $K_{x_i} \leftarrow K_{x_i} + (\cot\alpha_j + \cot\beta_j)(\mathbf{x}_j - \mathbf{x}_i)$ 
  end for
   $K_{x_i} \leftarrow \frac{K_{x_i}}{2\mathcal{A}_{x_i}}$ 
end for

```

threshold radius. This neighborhood definition is explained in below paragraph 3.2.2. The neighborhood (local window) radius determines the size of the detail which effect the frequency.

3D Neighborhood

The proposed method uses a scale parameter which defines the 3D neighborhood. Scale parameter enables to determine different variances to be considered as contribution to spatial frequency. The scale parameter is chosen to be %2 of the cubic bounding box for each mesh. Then, the definition of the 3D neighborhood with radius r for a vertex v_i is the set of neighboring vertices and edges:

- *Neighbor vertex* is a vertex whose distance to v_i is smaller or equal to radius r and is connected to a neighboring vertex or v_i . (in Fig. 3.5: blue vertices)
- *Neighbor edge* is an edge whose one end is a neighboring vertex and the other end is an "out vertex" whose distance to v_i exceeds radius r . These edges are treated as a vertex with curvature value equals to scale of the curvature value of the "out vertex". (in Fig. 3.5: yellow vertices)

The contribution of neighbor edge is:

$$K_{e_j} = K_j \frac{r}{\|\mathbf{v}_i - \mathbf{v}_j\|} \quad (3.4)$$

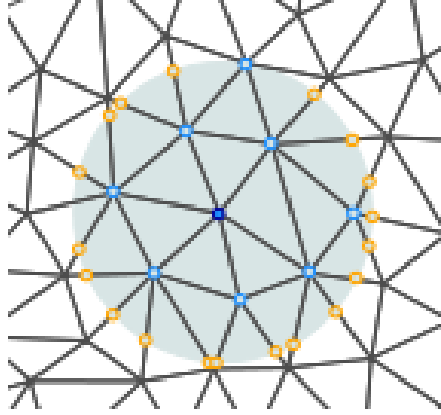


Figure 3.5: A local neighborhood of vertex

where v_j is the "out vertex" with e_j as the edge connecting it to a neighbor vertex. K_j is the curvature value at v_j .

Algorithm 3 Weighted Curvature Variance

```

for all  $x_i \in V(S)$  do
   $\mathcal{V}_{x_i} \leftarrow 0$ 
   $sn_{x_i} \leftarrow 0$ 
   $nc \leftarrow \#$  of  $x_j$  ( $x_j \in N_{local}x_i$ )
  for all  $x_j \in N_{local}x_i$  do
     $sn_{x_i} \leftarrow sn_{x_i} + n_{x_j}$ 
  end for
   $sn_{x_i} \leftarrow sn_{x_i}/nc$ 
  for all  $x_j \in N_{local}x_i$  do
     $x_jp \leftarrow$  projection of  $x_j$  to 2D plane of  $sn_{x_i}$ 
     $d_{ij} \leftarrow |x_i - x_jp|$ 
    if  $n_{x_j} \cdot n_{x_i} \neq 0$  then
       $\mathcal{V}_{x_i} \leftarrow \mathcal{V}_{x_i} + (d_{ij} * K_{x_j})$ 
    end if
  end for
   $\mathcal{V}_{x_i} \leftarrow \mathcal{V}_{x_i}/nc$ 
end for

```

3.2.3 3D Spatial Frequency Sensitivity Function

Contrast Sensitivity Function is a sensitivity threshold vs. spatial frequency function defined by experimental data, as described in section 2.3.1. Psychophysical

experiments show that CSF is highly sensitive to image size, noise, color, etc. due to the optics and adaptations of the eye. According to data gathered by the study of Ginsberg et al [12], CSF is formulated as

$$S(\rho, \theta, l, i^2, d, e) = P \cdot \min \left[S_1 \left(\frac{\rho}{r_a \cdot r_e \cdot r_\theta}, l, i^2 \right), S_1(\rho, l, i^2) \right] \quad (3.5)$$

where ρ is radial spatial frequency, θ is orientation, l is light adaptation, i is image size due to distance d and eccentricity e . r_a, r_e, r_θ are parameters for distance, eccentricity and orientation respectively. In order to use CSF, proper assumptions and calibrations should be established for an application. Viewing distance d can be different for each application but the observer's viewing distance is to remain in a certain range. We did not adapt to range fitting. Instead we have taken viewing distance as average viewing distance of users. Other parameter formulations are as follows:

$$\begin{aligned} r_a &= 0.856 \cdot d^{0.14} \\ r_e &= \frac{1}{1 + 0.24e} \\ r_\theta &= \left(\frac{(1 - ob)}{2} \right) \cos(4\theta) + \frac{(1 + ob)}{2} \end{aligned} \quad (3.6)$$

where $ob = 0.78$. Effects of the image size and light adaptation level leaves the formulation as:

$$\begin{aligned} S_1(\rho, l, i^2) &= ((3.23(\rho^2 i^2)^0.3)^5 + 1)^{-1/5} \cdot A_1 \epsilon \rho e^{B_1 \epsilon \rho} \sqrt{1 + 0.06 e^{B_1 \epsilon \rho}} \\ \text{where } A_1 &= 0.801 \left(\frac{1 + 0.7}{l} \right)^{-0.2} \\ \text{and } B_1 &= 0.3 \left(\frac{1 + 100}{l} \right)^{0.15} \end{aligned} \quad (3.7)$$

where l is light adaptation and i^2 is image area. Since our problem involves not a single rendered image, light adaptation is assumed to be a constant value. Equations 3.5, 3.6 and 3.7 are fitted to psychophysical data from study of Ginsberg et al [12] illustrated in Fig. 3.6.

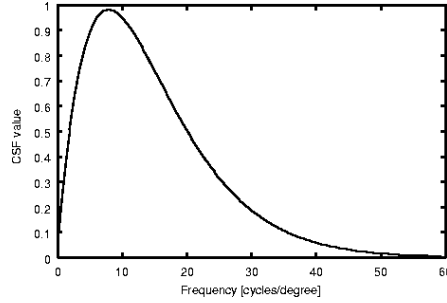


Figure 3.6: Typical Normalized CSF model used by our proposed method

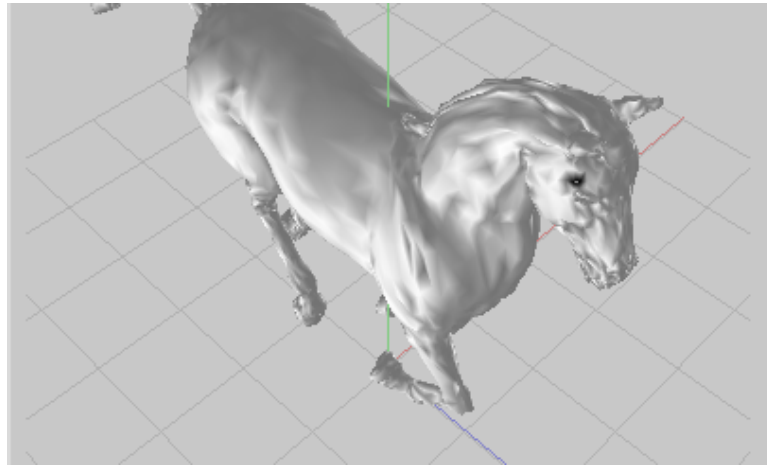


Figure 3.7: Output sensitivity map of a horse model

3.3 Visual Selectivity Model

Human Visual System is tuned to narrow ranges of spatial frequency and found out by neurophysiological studies of Hubel et al. [15]. This radial frequency selectivity can be modeled using Difference of Mesa filters. A Mesa filter is low-pass filter, with Gaussian boundary beyond a frequency f . The end result of the filter is a disc with blurry edges. The image can be generated with the formula:

$$m_0(r) = (\gamma/f)^2 \exp[-\pi(r\gamma/f)^2] * \Pi(r/2f) \quad (3.8)$$

where r is the distance of the point to the origin, Π is rectangular response which can be defined as 0 values except a given range where the response gets the value 1. The effect of Gaussian is obvious as blurry boundary of the disc. The level of blur is controlled by γ . f is defined as corner frequency and in our case it is propositioned to the average edge length.



Figure 3.8: A set of mesa filter generated with given equation 3.8

Difference of Mesa (DOM) Filters

Difference of mesa filters are calculated by subtraction of smaller filter from larger adjacent filter. Continuous subtraction of adjacent filters gives progressively smaller DOM filters. Each DOM filter equation is calculated as:

$$d_k(r) = m_k(r) - m_{k+1}(r) \quad (3.9)$$

where $m_i(r)$ is given by equation 3.8 Next, we apply DOM filters to vertex values from previous Spatial Frequency Sensitivity calculations. It is important to note that since a 3D model does not have a specific orientation at a given time, we have excluded fan filters from cortex transformation adaptation.

DOM Filters on 3D surfaces

We apply the set of DOM filters to each vertex at local window area.

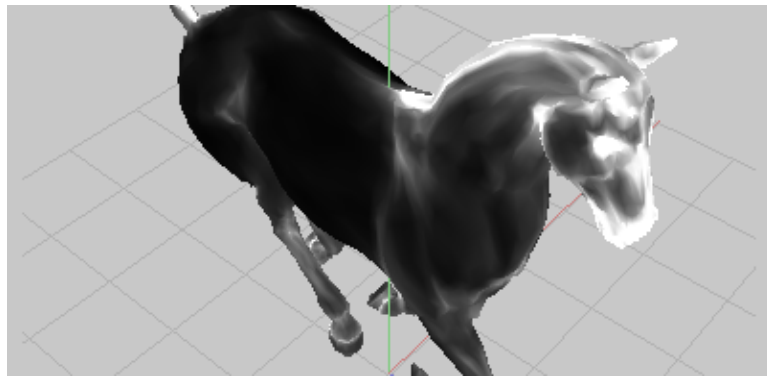


Figure 3.9: Selectivity map after DOM filter locally application to each vertex

3.4 Temporal Adaptations

The human visual system models use in not only spatial frequency but also temporal frequency as well. Weight of the neighboring curvatures indicate the rate that spatial frequency is effected by the variance. Kelly [18] has studied this effect by measuring threshold contrast for viewing traveling sine waves. Kelly's experiment used a special technique to stabilize the retinal image during measurements and therefore his models use the retinal velocity, the velocity of the target stimulus with respect to the retina.

The loss of sensitivity to high frequency spatial patterns in motion gives an opportunity to extend existing perceptually-based rendering techniques from static environments to dynamic environments. The eye, however, is able to track objects in motion to keep objects of interest in the foveal region where spatial sensitivity is at its highest. This tracking capability of the eye, also known as smooth pursuit, reduces the retinal velocity of the tracked objects and thus compensates for the loss of sensitivity due to motion. Therefore the temporal adaptation is processed as follows:

Algorithm 4 Temporal Adaptation

```

for all  $x_i \in V(S)$  do
   $vel_{x_i} \leftarrow \|\mathbf{x}_i - \mathbf{x}_j\|^2$ 
end for
for all  $x_i \in V(S)$  do
   $vel_{x_i} \leftarrow vel_{x_i} - \min(0.82 * vel_{x_i} + vel_{min}, vel_{max})$ 
   $G_{x_i} \leftarrow s_{x_i} / vel_{x_i}$ 
end for

```

Temporal Adjustments

First we calculate the 3D speed at each vertex by the distance difference between consecutive frames. This is then adapted with N_1 frames to reduce the erroneous mesh computations:

$$V_{it} = \|\mathbf{v}_{it} - \mathbf{v}_{i(t-1)}\| \quad (3.10)$$

$$V_{it} = \frac{V_{i(t-1)} + V_{it} + V_{i(t+1)}}{3} \quad (3.11)$$

Where V_{it} is the velocity value of vertex v_i at frame t .

Evidently, it is crucial that we compensate for smooth pursuit movements of the eye when calculating spatio-temporal sensitivity. The following equation describes a motion compensation heuristic proposed by Daly [7]:

$$v_R = v_I - \min(0.82v_I + v_{min}, v_{max}) \quad (3.12)$$

where v_R is the compensated retinal velocity, v_I is the physical velocity, v_{min} is 0.15 deg/sec (the drift velocity of the eye), v_{max} is 80 deg/sec (which is the maximum velocity that the eye can track efficiently). The value 0.82 accounts for Daly's data fitting that indicates the eye tracks all objects in the visual field with an efficiency of 82%.

Temporal Weight Factor

In section 2.3.3, temporal contrast sensitivity shown that with increased speed of the object, sensitivity to changes decreases accordingly. Using this analogy adjusted velocity values of the mesh are used as weight factors. The distance traversed by a vertex is assumed to linearly increase with growing value of speed. Thus the adjusted velocity values are used to directly as reverse weight factors and multiplied by Visual Selectivity results of the mesh.

At the end of this step 3D perception maps are fully computed and ready to be used for either difference computation or integrated into modification methods.

Chapter 4

Evaluation

To evaluate the fidelity of our perceptual quality estimation method, we opted for experiments. In this chapter, we explain the conducted experiments and discuss the results in detail. In section 4.1 we explain our experiment design and setup, and in Section 4.2 we present and analyze the experiment results.

4.1 Experimental Design

In this experiment, the correlation between the subjective evaluation results and the proposed method’s predictions are tested. Our fidelity measure for 3D quality on models was marking distortions that measures the perceived distortions by the subject. The experimental setup is an SDSCE category experiment (Simultaneous Double Stimulus for Continuous Evaluation).

In addition, we have computationally compared the relation between the modeled visual modules and change in correlation with respect to these modules. There are two main contributing modules of the method, spatial cortex and temporal adjustments modules.

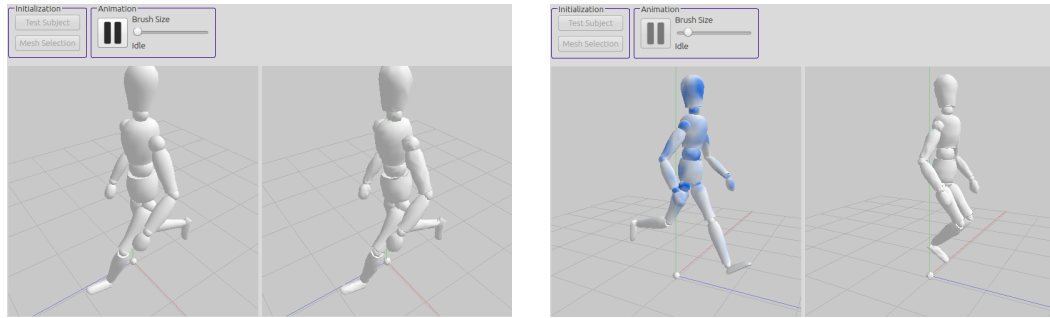
4.1.1 User Test Procedure

The reference meshes are prepared as 28 to 50 frame long animated models. For modified versions, random noise offset is applied to each frame of a reference model. Test subjects were shown both the reference and modified versions simultaneously and were able to manipulate the viewing point by means of rotation and zooming. By problem definition, viewing 3D mesh in a static manner would defeat the purpose, thus we have conducted evaluation process after the animation was stopped and test mesh was removed from the viewing panel. This brings unwanted memorizing strain to the viewer. However, we have conducted a survey after the experiment and 82% of the subjects stated they did not feel restrained from memorizing. Remaining subjects stated they felt that memorization affected their response below 5%.

Marking

For marking on modified mesh, the viewer was supplied with a simple mark tool with tip intensity. Paint tool and view-point manipulation enabled the viewer to correctly locate and mark the perceived distortions. The marked vertex patches were represented as color changes on the mesh. Figure 4.1 shows the viewer test setup. On left panel, the reference model shown to the viewers to prevent drawbacks of memorizing a complex 3D form. On the right panel the modified mesh was given and the viewer can paint on faces of the mesh by mark tool. Scale of tip was represented as a bar on top and viewer was able to control the animation by using a button widget.

At the start of the experiments the viewers were only given the instruction as “Distortion on mesh was defined by spatial artifacts. Consider relative scale of distortions and mark the distortions accordingly using the intensity tool”.



(a) The experiment setup and environment at viewing stage. Both images are in animation and interaction is simultaneous.

(b) Evaluation stage of experiment with reference mesh without animation and marking is enabled (left mesh panel). Test mesh continue animation (right mesh panel). Interaction is simultaneous.

Figure 4.1: Experimental setup for viewing stage and marking stages

4.1.2 Setup

Experimental environment setup has a significant impact on subjective results in computer generated scene tests. Therefore parameters of the experiment was carefully considered. Each parameter is explained below.

- *Lighting*: Type, position and direction of the lighting are significant factors in experimental setup. We have chosen stationary left-above, center directed lighting [32].
- *Background*: We have adopted chess lines design on x-z plane for a sense of up vector of the mesh and also to prevent overestimation of the mesh boundaries.
- *Materials and Shading*: To prevent highlighting effects and accentuate distortions unpredictably, we have chosen smooth-shaded rendering in experiments.
- *Animation and Interaction*: Free-viewpoint was enabled to the viewers for interaction. Animation was used by the nature of the problem. Furthermore, since inspection of the mesh during paused state was contradictory to experiment's purpose, evaluation of the mesh was conducted after the animation

was stopped and test mesh was removed from the test environment.

- *Stimuli order*: Each modified and reference model combination was shown successively allowing for more accurate comparisons.

4.1.3 Subjects

For the psychovisual experiments, 17 subjects participated with different level of computer abilities. Most of the subjects were moderate computer the viewers with knowledge on computer science but with limited background on computer graphics field. All of the participants were tested with every animated model.

4.1.4 Data

We have 3 reference meshes with two modified versions for each, totaling 6 mesh pairs. Statistics of these meshes are explained in an Table 4.1 below.

	M_{D1}	M_{D2}	M_{H1}	M_{H2}	M_{S1}	M_{S2}
$\#ofV(M)$	3423	3423	8321	8321	8431	8431
$\overline{ e_M }$.01015	.00981	.01208	.01170	.01336	.01290
$\overline{d(f_{M_0}, f_{M_1})}$.00099	.00059	.00124	.00073	.00136	.00080

Table 4.1: Statistics of modified meshes; vertex count, mean edge length and mean face distortions

M_{D1} , M_{D2} , M_{H1} , M_{H2} , M_{S1} and M_{S2} are modified meshes, and first line of the table represents the vertex count of each mesh. The second row is average edge length and third row is average distance between faces of original and modified mesh. As can be seen from Table 4.1, distortions on the faces are not significantly larger than average edge length.

4.2 Results & Analysis

The marked meshes are stored as vertex color maps. User response for a modified mesh was a set of vertices with color values between $[0 \dots 1]$. Sample viewer responses are shown in figure 4.2c, 4.2d, 4.2e, 4.3c, 4.3d and 4.3e for mesh pairs shown in figure 4.2a and 4.3a respectively. To calculate a unified subjective response for each mesh we calculate a mean subjective response.

For each animated model, mean subjective response is computed per vertex given by the equation :

$$\mu(v_{i,M'}) = \frac{\sum_{s=0}^N R_s(v_{i,M'})}{N} \quad (4.1)$$

where N is the test subject count for the mesh M' . $R_{s,f}(v_{i,M'})$ represents the given response to a single vertex, mesh and subject combination.

Next, the proposed method is computed for each mesh pair. Sample evaluations are shown in Figures 4.3b and 4.2b for mesh pairs 4.3a and 4.2a respectively.

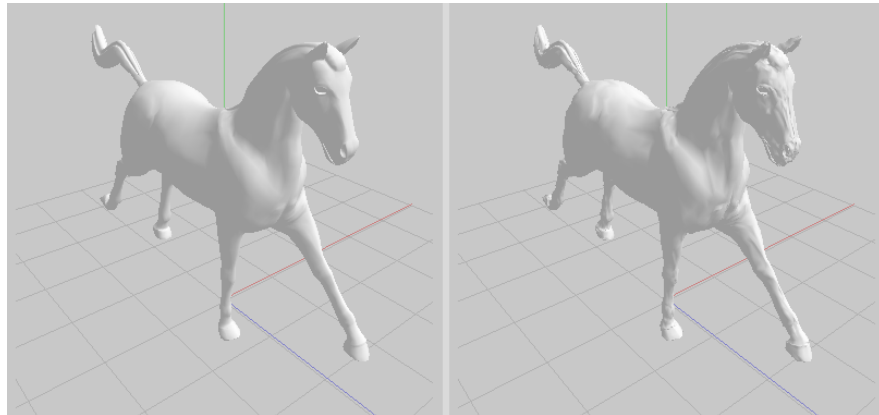
Analysis

The relationship between the viewers responses and quality estimations of each conditions is analyzed using correlation method. We opted for Pearson's product-moment correlation coefficient r . This method is suitable for measuring correlation between two variables, giving a value between $[-1 \dots 1]$. If the resulting value of r is close to 1 there exists a linear correlation, meaning the variables' correlation is higher. The formulation for Pearson's correlation coefficient r is given in equation.

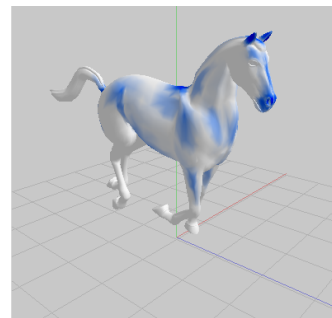
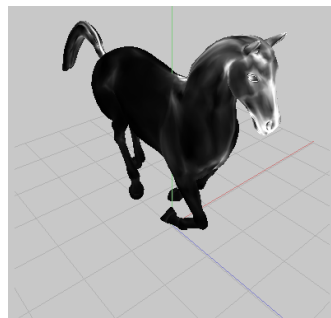
$$r = \frac{1}{n-1} \sum_{i=1}^n \left(\frac{X_i - \bar{X}}{s_x} \right) \left(\frac{Y_i - \bar{Y}}{s_y} \right) \quad (4.2)$$

where \bar{X} is sample mean and s_x is sample standart deviation.

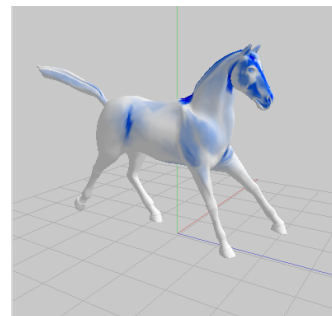
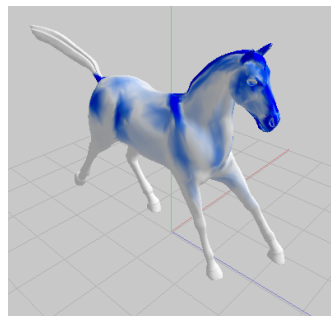
Our variables are method evaluation values and mean subjective responses. Each variable spans vertices, therefore, sample size is equal to number of vertices



(a) Reference and modified meshes

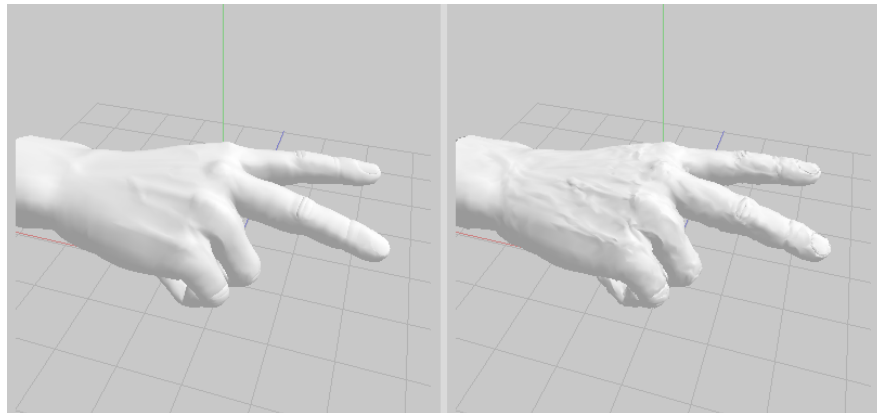


(b) Difference map of horse mesh pair (c) User Evaluation No. 1

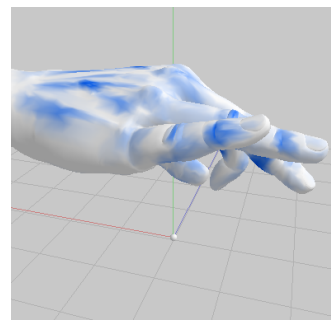
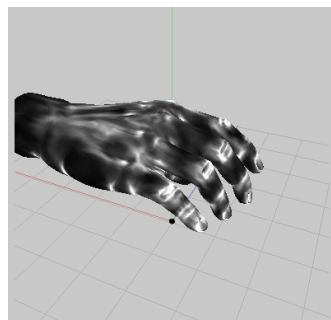


(d) User Evaluation No. 2 (e) User Evaluation No. 3

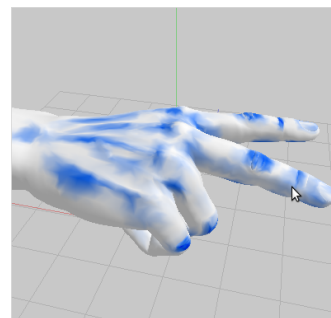
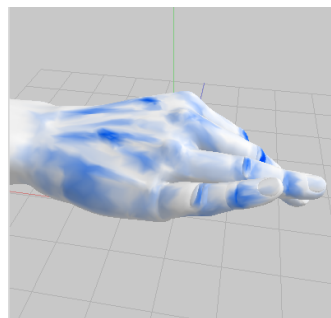
Figure 4.2: Horse mesh quality assessment experiment: Sample viewer evaluations, difference map and visual comparison of reference and test mesh is given



(a) Reference and modified meshes



(b) Difference map of hand mesh pair (c) User Evaluation No. 1



(d) User Evaluation No. 2 (e) User Evaluation No. 3

Figure 4.3: Hand mesh quality assessment experiment: Sample viewer evaluations, difference map and visual comparison of reference and test mesh is given

for a mesh. Thus, total number of samples is 40350.

The correlation between method evaluation values and mean subjective responses is 0.28 and correlation graph is shown in Figure 4.4

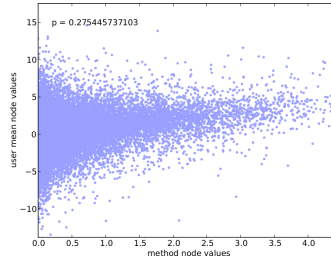
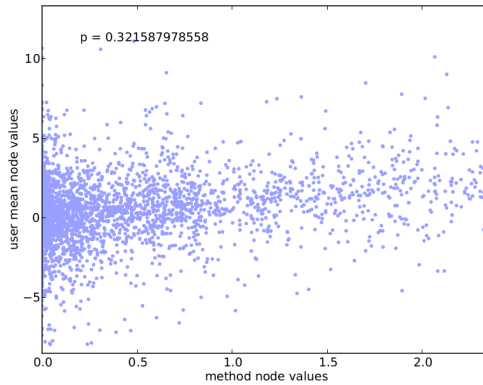
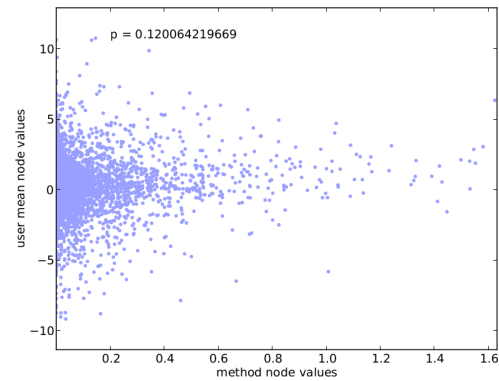


Figure 4.4: Correlation map for all samples combined

Given the proposed method gives an estimation and 3D marking tool limitations, correlation between our proposed method's estimates and the viewer responses are high. Furthermore, the correlation graph indicates that our proposed method accurately estimates high distortion areas where values are higher. Lower distortions are harder to identify by the viewers and therefore there is a greater inconsistency between the viewer responses and method estimation. This effect is better observed when correlation is measured separately for each model.

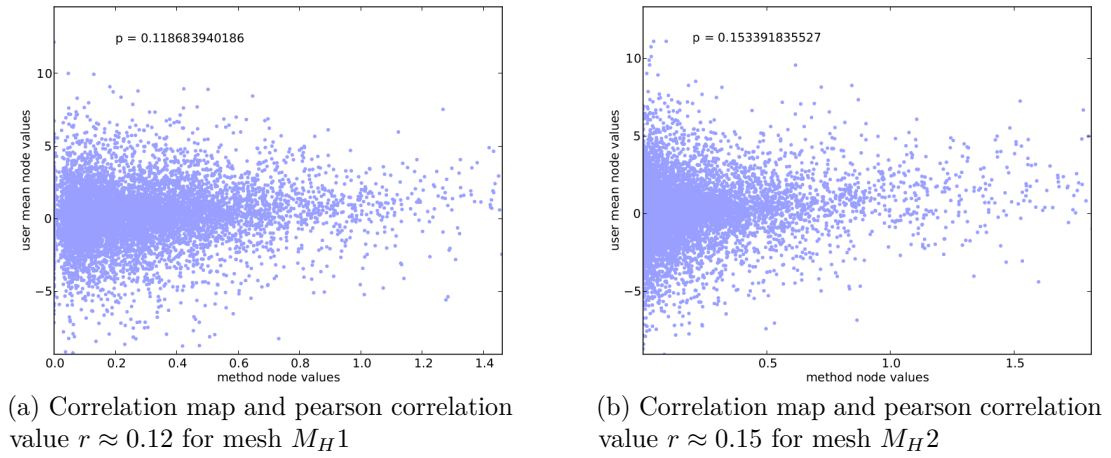
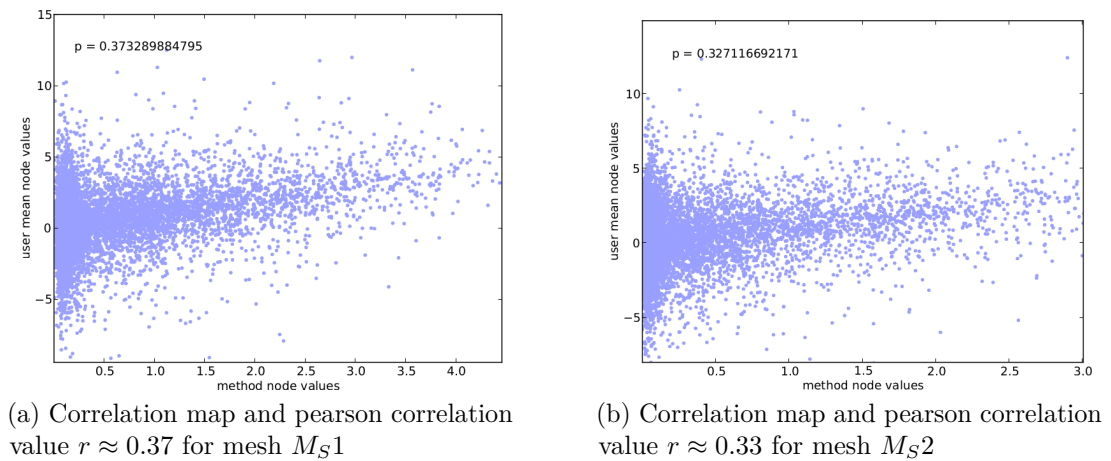


(a) Correlation map and pearson correlation value $r \approx 0.32$ for mesh M_D1



(b) Correlation map and pearson correlation value $r \approx 0.12$ for mesh M_D2

Figure 4.5: Correlation map for each modified mesh of *Doll* is given.

Figure 4.6: Correlation map for each modified mesh of *Hand* is given.Figure 4.7: Correlation map for each modified mesh of *Horse* is given.

Chapter 5

Conclusion

In this work, we proposed a quality assessment framework with emphasis on perception combining spatial and temporal aspects of seeing. Our system works on 3D animated meshes but can also be used for static 3D mesh pairs. To create an object-space solution while standing by perceptual nature of the problem, we have devised a method for estimation of image-space attributes using solely geometrical information. In addition, we have applied image space filters to surfaces in 3D using HVS visual selectivity models as a guide. Lastly, temporal information of animated models was adjusted to visual system adaptations and limitations for more accurate representation of a mesh from a perceptual point of view. To test our method, we have conducted subjective evaluations of modified models and measured the correlation between results from the proposed model and by user evaluation. During user tests, the viewers were asked to mark the defects on 3D mesh by painting. Evaluation results showed that our model was successful at prediction of detectability of artifacts in animated 3D models.

To further represent a quality estimation, other perceptual contributors can be integrated. One important contributing factor to perceptual quality would be saliency. Saliency and spatial frequency sensitivity are two opposite effects of similar structural phenomena. Addition of saliency consideration would reduce misleading quality increase caused by spatial frequency. It is worth noting that subjects usually marked only easily visible regions such as sides and top of the

mesh, and needed reminding of examining the mesh from hard to see angles such as below. Thus, 3D meshes with an up direction can benefit from point-of-view reductions in computation.

Overall, our proposed method computed suitable perceptual results to the given mesh pair and upon conducting the user test, strong correlations between automated results and viewers' responses were observed. Thus, we conclude that the method provides a suitable solution for estimating the perceived quality of animated 3D meshes.

Bibliography

- [1] C. Blakemore and F. W. Campbell. On the existence of neurones in the human visual system selectively sensitive to the orientation and size of retinal images. *J Physiol*, 203(1):237–260, July 1969.
- [2] M. R. Bolin and G. W. Meyer. A perceptually based adaptive sampling algorithm. In *Proceedings of the 25th annual conference on Computer graphics and interactive techniques*, SIGGRAPH '98, pages 299–309, New York, NY, USA, 1998. ACM.
- [3] M. Brewer, L. Diachin, P. Knupp, T. Leurent, and D. Melander. The Mesquite mesh quality improvement toolkit. *Proc. of 12th IMR*, pages 239–250, 2003.
- [4] P. Cignoni, C. Rocchini, and R. Scopigno. Metro: Measuring Error on Simplified Surfaces. *Comput. Graph. Forum*, 17(2):167–174, 1998.
- [5] M. Corsini, E. Gelasca, T. Ebrahimi, and M. Barni. Watermarked 3-D mesh quality assessment. *Multimedia, IEEE Transactions on*, 9(2):247–256, 2007.
- [6] S. Daly. The visible differences predictor: an algorithm for the assessment of image fidelity. In A. B. Watson, editor, *Digital images and human vision*, chapter The visible differences predictor: an algorithm for the assessment of image fidelity, pages 179–206. MIT Press, Cambridge, MA, USA, 1993.
- [7] S. Daly. Engineering observations from spatiovelocity and spatiotemporal visual models. In *Human Vision and Electronic Imaging III*, volume 3299, pages 180–191. SPIE, 1998.

- [8] H. DE LANGE DZN. Research into the dynamic nature of the human fovea-cortex systems with intermittent and modulated light. II. Phase shift in brightness and delay in color perception. *J Opt Soc Am*, 48(11):784–789, Nov 1958.
- [9] J. A. Ferwerda, P. Shirley, S. N. Pattanaik, and D. P. Greenberg. A model of visual masking for computer graphics. In *Proceedings of the 24th annual conference on Computer graphics and interactive techniques*, SIGGRAPH '97, pages 143–152, New York, NY, USA, 1997. ACM Press/Addison-Wesley Publishing Co.
- [10] M. Garland and P. Heckbert. *Fast polygonal approximation of terrains and height fields*. Citeseer, 1995.
- [11] E. Gelasca, T. Ebrahimi, M. Corsini, and M. Barni. Objective evaluation of the perceptual quality of 3D watermarking. In *Image Processing, 2005. ICIP 2005. IEEE International Conference on*, volume 1, pages I–241. IEEE, 2005.
- [12] A. P. Ginsberg and D. W. Evans. Rapid Measurement of Contrast Sensitivity Using a New Contrast Sensitivity Vision Test Chart System: Initial Population Data. *Proceedings of the Human Factors and Ergonomics Society Annual Meeting*, 28(2):123–127, 1984.
- [13] A. Guézic. Surface simplification with variable tolerance. In *Second Annual Intl. Symp. on Medical Robotics and Computer Assisted Surgery (MR-CAS'95)*, pages 132–139, 1995.
- [14] S. Howlett, J. Hamill, and C. O'Sullivan. An experimental approach to predicting saliency for simplified polygonal models. In *Proceedings of the 1st Symposium on Applied perception in graphics and visualization*, APGV '04, pages 57–64, New York, NY, USA, 2004. ACM.
- [15] D. H. HUBEL and T. N. WIESEL. Receptive fields, binocular interaction and functional architecture in the cat's visual cortex. *J. Physiol. (Lond.)*, 160:106–154, Jan 1962.
- [16] R. Jones. A self-organizing mesh generation program. *Journal of Pressure Vessel Technology*, 96:193, 1974.

- [17] Z. Karni and C. Gotsman. Spectral compression of mesh geometry. In *Proceedings of the 27th annual conference on Computer graphics and interactive techniques*, pages 279–286. ACM Press/Addison-Wesley Publishing Co., 2000.
- [18] D. Kelly. Motion and vision. II. Stabilized spatio-temporal threshold surface. *JOSA*, 69(10):1340–1349, 1979.
- [19] S.-J. Kim, S.-K. Kim, and C.-H. Kim. Discrete Differential Error Metric for Surface Simplification. In *Pacific Conference on Computer Graphics and Applications*, pages 276–283. IEEE Computer Society, 2002.
- [20] P. Knupp. Winslow smoothing on two-dimensional unstructured meshes. *Engineering with Computers*, 15(3):263–268, 1999.
- [21] G. Lavoué. A local roughness measure for 3D meshes and its application to visual masking. *ACM Trans. Appl. Percept.*, 5:21:1–21:23, February 2009.
- [22] C. Lee, A. Varshney, and D. Jacobs. Mesh saliency. In *ACM SIGGRAPH 2005 Papers*, pages 659–666. ACM, 2005.
- [23] B. Li, G. W. Meyer, and R. V. Klassen. A Comparison of Two Image Quality Models. In *Proceedings of SPIE*, 1998.
- [24] P. Longhurst and A. Chalmers. User Validation of Image Quality Assessment Algorithms. In *Proceedings of the Theory and Practice of Computer Graphics 2004 (TPCG'04)*, pages 196–202, Washington, DC, USA, 2004. IEEE Computer Society.
- [25] K. Low and T. Tan. Model simplification using vertex-clustering. In *Proceedings of the 1997 symposium on Interactive 3D graphics*, pages 75–ff. ACM, 1997.
- [26] J. Lubin. *A Visual Discrimination Model for Imaging System Design and Evaluation*. World Scientific, 1995.
- [27] D. Luebke, B. Watson, J. D. Cohen, M. Reddy, and A. Varshney. *Level of Detail for 3D Graphics*. Elsevier Science Inc., New York, NY, USA, 2002.

- [28] M. Meyer, M. Desbrun, P. Schröder, and A. H. Barr. Discrete Differential-Geometry Operators for Triangulated 2-Manifolds, 2002.
- [29] Y. Pan, L. I. Cheng, and A. Basu. Quality metric for approximating subjective evaluation of 3-D objects. *IEEE Transactions on Multimedia*, 7(2):269–279, 2005.
- [30] G. Ramanarayanan, J. Ferwerda, B. Walter, and K. Bala. Visual equivalence: towards a new standard for image fidelity. In *ACM SIGGRAPH 2007 papers*, SIGGRAPH '07, New York, NY, USA, 2007. ACM.
- [31] M. Ramasubramanian, S. N. Pattanaik, and D. P. Greenberg. A perceptually based physical error metric for realistic image synthesis. In *Proceedings of the 26th annual conference on Computer graphics and interactive techniques*, SIGGRAPH '99, pages 73–82, New York, NY, USA, 1999. ACM Press/Addison-Wesley Publishing Co.
- [32] B. E. Rogowitz and R. H. E. Are Image Quality Metrics Adequate to Evaluate the Quality of Geometric Objects? In *Human Vision and Electronic Imaging*, 2001.
- [33] J. Rossignac and P. Borrell. *Multi-resolution 3D approximations for rendering complex scenes*. IBM Research Division, TJ Watson Research Center, 1992.
- [34] R. Tipton. Grid optimization by equipotential relaxation. *unpublished*, Lawrence Livermore National Laboratory, 1990.
- [35] Z. Wang, H. R. Sheikh, and A. C. Bovik. No-Reference Perceptual Quality Assessment of JPEG Compressed Images. pages 477–480, 2002.
- [36] A. B. Watson. The cortex transform: rapid computation of simulated neural images. *Comput. Vision Graph. Image Process.*, 39(3):311–327, Sept. 1987.
- [37] B. Watson, A. Friedman, and A. McGaffey. Measuring and predicting visual fidelity. In *Proceedings of the 28th annual conference on Computer graphics and interactive techniques*, SIGGRAPH '01, pages 213–220, New York, NY, USA, 2001. ACM.

- [38] J. Wu, S. Hu, J. Sun, and C. Tai. An effective feature-preserving mesh simplification scheme based on face constriction. *pg*, page 0012, 2001.